Physics – Uspekhi **60** (5) 509 – 533 (2017)

INSTRUMENTS AND METHODS OF INVESTIGATION PACS numbers: **28.52. – s**, **52.50. – b**, 52.55. Jd

Gas dynamic trap: experimental results and future prospects

A A Ivanov, V V Prikhodko

DOI: https://doi.org/10.3367/UFNe.2016.09.037967

Contents

Abstract. The gas dynamic trap (GDT) is a version of a magnetic mirror with a long mirror-to-mirror distance far exceeding the effective mean free path of ion scattering into the loss cone, with a large mirror ratio ($R \sim 100$; $R = B_{\max}/B_{\min}$ is the ratio of magnetic field inductions at the mirror and at the trap center) and with axial symmetry. Under these conditions, in contrast to a conventional magnetic mirror, the plasma confined in a GDT is isotropic and Maxwellian. The plasma loss rate through the ends is governed by a set of simple gas dynamic equations; hence, the name of the device. The plasma lifetime in a GDT is on the order of LR/V_{Ti}, where L is the mirror-to-mirror distance, and V_{Ti} is the ion thermal velocity. Thus, increasing both the length of the device and the mirror ratio can, in principle, make the plasma lifetime sufficient for fusion applications. This paper discusses plasma confinement and heating results from the Novosibirsk GDT facility and examines prospects for using GDTs to develop a high-flux volumetric neutron source for fusion material testing and for driving subcritical fission reactors.

Keywords: gas dynamic trap, fusion neutron source, magnetic mirror

A A Ivanov Budker Institute of Nuclear Physics,
Siberian Branch of the Russian Academy of Sciences,
prosp. Akademika Lavrent'eva 11, 630090 Novosibirsk,
Russian Federation;
Novosibirsk State University,
ul. Pirogova 2, 630090 Novosibirsk, Russian Federation
E-mail: A.A.Ivanov@inp.nsk.su
V V Prikhodko Budker Institute of Nuclear Physics, Siberian Branch of the Russian Academy of Sciences,
prosp. Akademika Lavrent'eva 11, 630090 Novosibirsk,
Russian Federation;
Novosibirsk State University,
ul. Pirogova 2, 630090 Novosibirsk, Russian Federation;
Nuclear Safety Institute, Russian Academy of Sciences (IBRAE),
ul. B Tul'skaya 52, 115191 Moscow, Russian Federation
E-mail: V.V.Prikhodko@inp.nsk.su

Received 4 July 2016, revised 20 September 2016
Uspekhi Fizicheskikh Nauk **187** (5) 547 – 574 (2017)
DOI: https://doi.org/10.3367/UFNr.2016.09.037967
Translated by Yu V Morozov; edited by A Radzig

1. Introduction and basic principles of the theory of open magnetic traps

The present study deals with gas dynamic trap physics. For completeness, it seems opportune to recall the fundamental principles on which open plasma confinement systems are based as exemplified by the gas dynamic trap (GDT), making up the central topic of the forthcoming discussion. A magnetic mirror trap ('probkotron') — topologically different from tokamaks and stellarators — represents the simplest type of linear magnetic trap proposed in 1954 by G I Budker (USSR) and, independently, by R F Post (USA) [1, 2]. In such devices, the plasma is confined by a transverse magnetic field, and its free longitudinal flow is limited by particle reflection from high magnetic field regions, so-called magnetic mirrors (Fig. 1). The reflection of the particles proceeds due to the law of conservation of energy and the constant magnetic moment of the 'Larmor circle' of particles, which is an adiabatic invariant when the particles travel in a weakly nonuniform magnetic field:

$$\mu = \frac{mv_{\perp}^2}{2B} .$$

Here, B is the magnetic field induction, m is the particle mass, $v_{\perp}$ is the particle velocity across the magnetic field. The mirrors reflect particles with a high enough transverse velocity in the trap center, so that the following condition is

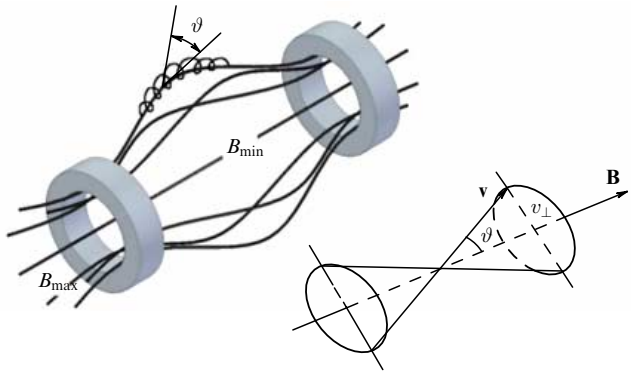

Figure 1. Simplest magnetic mirror trap (probkotron).

fulfilled:

$$\mathcal{E} = \frac{mv_{\|}^2}{2} + \mu B_{\min} \leqslant \mu B_{\max} ,$$

where $\mathcal{E}$ is the total energy of a particle, $v_{\|}$ is the particle velocity along the magnetic field, and $B_{\min}$ and $B_{\max}$ are the magnetic field values in the trap center and in the magnetic mirror, respectively (the influence of electrical potential is ignored here).

In the velocity space ($v_{\|}$, $v_\perp$), the plasma confinement region is located outside the cone with the vertex angle $\vartheta = \arcsin 1/\sqrt{R}$, where $R = B_{\max}/B_{\min}$ is the mirror ratio. The transit of ions from the confinement region to the loss cone and their eventual escape from the trap along the magnetic field occur in a time on the order of Coulomb ion collisions between themselves:

$$\tau_{ii} = \frac{1}{\sqrt{2}\pi} \frac{\sqrt{m_i T_i^3}}{e^4 \Lambda_i n_i} ,$$

where e is the elementary charge (we are dealing with hydrogen plasma), m_i, T_i, and n_i are the ion mass, temperature, and number density, respectively, and Λ_i is the Coulomb logarithm. Electron scattering and escape into the loss cone occur, at the same energy, $\sqrt{m_i/m_e}$ times faster (m_e is the electron mass). As a result, an electric field is generated in the plasma that equalizes electron and ion fluxes into the mirrors, thus leaving the plasma quasineutral. The arising potential is called ambipolar. Electrons trapped in a potential well a few temperatures deep exhibit isotropic and Maxwellian velocity distribution. The ambipolar potential profile along a magnetic field line is defined for Maxwellian electrons by the Boltzmann formula:

$$e\varphi(l) = T_e \ln\left(n_e(l)\right) + \text{const} ,$$

where φ is the potential, T_e and n_e are the electron temperature and density, and l is the coordinate along the magnetic field line. The ambipolar electrical field

$$E_{\|} = -\frac{\partial\varphi}{\partial l} = -\frac{T_e}{en}\frac{\partial n}{\partial l}$$

pushes ions out of the trap if plasma density decreases toward the magnetic mirror, with their longitudinal motion being described by the relation

$$\frac{m_i v_{\|}^2}{2} = \mathcal{E} - U_{\text{eff}} ,$$

where $\mathcal{E} = m_i v^2/2 + e\varphi$ is the total ion energy, and $U_{\text{eff}} = e\varphi + \mu B$ is the effective potential energy, frequently referred to as the Yushmanov potential [3]. The ion loss rate from the trap is a function of the ratio of ion energy to the Yushmanov potential maximum, depending, in turn, on the density profile. The exact solution to this problem is possible, in general, only by numerical methods, because the density profile depends on two factors, viz. the ion velocity distribution function and the ion confinement region in the velocity space. To recall, the ambipolar potential drop is small compared with the ion energy, when electron temperature is not very high, as is frequently the case in magnetic mirror trap experiments. Under these conditions, the above estimate of the ion loss rate from the trap remains correct to an order of magnitude.

Not infrequently, a model is applied for simplicity in which the magnetic field is assumed to be constant in the trap but increase jumpwise in the mirror, while the entire ambipolar potential drop is accumulated in the mirror (the rectangular magnetic well model). In this approximation, plasma as a whole acquires a positive potential φ_0 such that the boundary of the ion confinement region in the velocity space turns into a two-cavity hyperboloid:

$$v_{\|}^2 - \frac{v_\perp^2}{R-1} = \frac{2e\varphi_0}{m_i(R-1)} .$$

For impurity ions, the right-hand part of this relationship should be multiplied by impurity charge Z. In the case of high-charge ions, it leads to their loss from the trap for practically a single transit between the mirrors. Low-charge impurity ions leave the trap equally fast due to both the extension of the loss hyperboloid and the enhancement of scattering rate on the bulk plasma ions. It can be concluded that a specific mechanism operates in open magnetic traps to purify plasma from heavy admixtures. Their accumulation in closed traps may be a cause of serious difficulties.

If electron temperature is sufficiently low and the influence of the ambipolar potential insignificant, the solution of the kinetic equation indicates that an increase in the mirror ratio results in a very slow (logarithmic) growth of ion confinement time:

$$\tau_{\text{kin}} \approx 0.4\tau_{ii} \ln R . \qquad (1)$$

This means that increasing the mirror ratio does not appreciably prolong the ion lifetime in a trap. Numerical calculations show that the value of Q (magnification factor for the power introduced into an open trap-based fusion reactor) can be close to unity at the very best [4].

Due to the existence of the loss cone, the plasma confined in the probkotron is always characterized by anisotropic distribution of ions over velocities. In the Cartesian coordinate system, the momentum flux tensor has the form

$$P_{\alpha\beta} = p_\perp\left(\delta_{\alpha\beta} - \frac{B_\alpha B_\beta}{B^2}\right) + p_{\|}\frac{B_\alpha B_\beta}{B^2} .$$

This expression disregards nondiagonal elements of the tensor proportional to the ratio squared of the ion Larmor radius to the plasma radius. The nondiagonal elements describe plasma viscosity and, as a rule, do not disturb equilibrium. Longitudinal and transverse plasma pressures are usually very different in open magnetic plasma trap

machines. For example, the generation and maintenance of plasma by injecting neutral beams across the magnetic field in the trap equatorial plane may lead to creating conditions under which $p_\perp \gg p_{||}$.

The equation describing plasma equilibrium state in a magnetic field can be written down as

$$\frac{\partial}{\partial x_\beta}\left(P_{\alpha\beta} + T_{\alpha\beta}\right) = 0\,,$$

$$T_{\alpha\beta} = p_\mathrm{m}\left(\delta_{\alpha\beta} - \frac{B_\alpha B_\beta}{B^2}\right) - p_\mathrm{m}\,\frac{B_\alpha B_\beta}{B^2}\,, \quad p_\mathrm{m} = \frac{B^2}{8\pi}\,,$$

where $T_{\alpha\beta}$ is the Maxwellian tensor of magnetic field tension, and p_m is the magnetic pressure. Plasma pressure in equilibrium distorts the vacuum magnetic field, which leads to the appearance of a compensation force $(1/c)\,[\mathbf{j}\,\mathbf{B}]$ generated by the plasma current. Assuming that $p_\perp \approx p_{||} \approx p$ makes it possible to introduce a dimensionless parameter $\beta = p/p_\mathrm{m}$ to describe equilibrium. Clearly, this parameter cannot be much higher than unity if plasma pressure is to be counterbalanced by magnetic pressure. What is the maximum β value of the plasma in a given magnetic configuration? This problem requires numerical calculations to be solved, especially for not an axisymmetric system. However, the form of the equilibrium equation suggests that the maximum β value must be of the order of unity provided the system has no small parameters. This conclusion applies to short probkotrons with the plasma transverse size close to the mirror-to-mirror distance and holds equally well for long axisymmetric magnetic confinement devices in which the mirror-to-mirror distance is much greater than the plasma transverse dimension [5].

The equation describing plasma equilibrium state along the magnetic field reduces to the expression $\partial p_{||}/\partial B = (p_{||} - p_\perp)/B$, which means that longitudinal pressure drops in the direction to the mirror if it is lower than the transverse one, i.e., the plasma confined in the open magnetic mirror trap is anisotropic.

There are a variety of plasma instabilities responsible for enhanced plasma losses in open traps with simple axially symmetric magnetic field. The most dangerous of them is interchange or flute instability.

Developing plasma boundary perturbations are reminiscent of flutes stretched along magnetic field lines (Fig. 2), so-called magnetohydrodynamic (MHD) perturbations. The cause of instability is the azimuthal drift of electrons and ions in opposite directions in the nonuniform radially decaying magnetic field of the trap. The drift results in charge separation in the perturbation field, plasma polarization in the flutes, and its radial outflow. Instability is unrelated to any feature of the ion velocity distribution function and develops very rapidly, so that the plasma is lost transversely for a time commensurate with the time of ion flight along the trap.

Figure 2. Perturbation of plasma boundary associated with the development of flute instability. Arrows show main magnetic field lines.

The equation for the plasma magnetic field in the MHD approximation has the form

$$\frac{\partial \mathbf{B}}{\partial t} = \mathrm{rot}\,[\mathbf{v}\,\mathbf{B}] + \frac{c^2}{4\pi\sigma}\,\nabla^2\mathbf{B}\,,$$

where v and σ are plasma velocity and conductivity, respectively, and c is the speed of light. If plasma conductivity is high enough, the last term in the equation can be disregarded, reducing it to

$$\frac{\partial \mathbf{B}}{\partial t} = \mathrm{rot}\,[\mathbf{v}\,\mathbf{B}]\,.$$

This equation is referred the 'freezing-in' condition. In such an approximation, the plasma is 'frozen' in the magnetic field; in other words, the field lines move together with the plasma and the quantity B/ρ (where ρ is the plasma density) changes at each point in proportion to the stretching of the respective 'liquid' line. If velocity perturbation is expressed through the plasma displacement, $\mathbf{v} = \partial\xi/\partial t$, magnetic field variations can be related to the displacement vector: $\delta\mathbf{B} = \mathrm{rot}\,[\xi\mathbf{B}]$. The most dangerous perturbations have the form of 'blades' thin in the azimuthal direction that expand the magnetic field without perturbation of the magnetic energy: $[\xi\mathbf{B}] = \psi$ (with $\delta\mathbf{B} = 0$), where ψ is a certain scalar function.

It was supposed that MHD instability might be suppressed using, in addition to the main trap field, the quadrupole magnetic field generated in the simplest case by a system of alternately directed currents parallel to the trap axis ('Ioffe bars') [6]. This allows instability to be stabilized once the additional quadrupole field is sufficiently high. In particular, stability is achieved when the magnetic field modulus increases in all directions from the trap center, which leads to a change in the directions of ion and electron azimuthal drifts, so as to prevent a growth of perturbations (the 'minimum-B' principle). A few more analogous configurations proposed in later publications are characterized by a relatively greater minimal field volume. At the same time, when stabilizing MHD instability it will only suffice that ions and electrons in the emerging flute (on average over its section) drift in the required direction, because, in the approximation being considered, plasma conductivity along the magnetic field is high enough and the potential becomes levelled along the magnetic field lines. In this case, stabilization is reached if the total azimuthal current flowing through the flute does not heighten plasma polarization. The density of the current generated by particles' drift in a nonuniform magnetic field is defined as

$$j_\perp = ne(v_{\perp\mathrm{i}} - v_{\perp\mathrm{e}}) = \frac{c\kappa}{B}\left(P_\perp + P_{||}\right),$$

where κ is the curvature of a magnetic line, and $P_\perp = p_\perp$ and $P_{||} = p_{||} + \rho v_{||}^2$ are components of the momentum flux tensor expressed through plasma pressure and velocity, respectively. (Notice that mean azimuthal velocities of ions and electrons, $v_{\perp\mathrm{i}}$ and $v_{\perp\mathrm{e}}$, are different, whereas longitudinal velocities are equal: $v_{||\mathrm{i}} = v_{||\mathrm{e}} = v_{||}$.) The displacements in the flutes depend on the longitudinal coordinate along a magnetic field line as $\xi = \xi_0(r_0 B_0/rB)$, while the subscript '0' denotes quantities in

the central plane. Accordingly, an azimuthal current density expressed as

$$j_\perp \xi \, \mathrm{d}l = \frac{c\kappa}{B} \left(P_\perp + P_\parallel\right) \xi_0 \, \frac{r_0 B_0}{rB} \, \mathrm{d}l$$

flows across the flute section.

Integrating this expression along the magnetic field line yields the stability criterion [5, 7]

$$\int \left(p_\perp + p_\parallel + \rho v_\parallel^2\right) \frac{\kappa}{B^2 r} \, \mathrm{d}l \geqslant 0 \,. \tag{2}$$

This approach was applied in the original study [8] on the assumption that the contribution of the plasma between the magnetic mirrors where the curvature is unfavorable for stability can be compensated for by its contribution behind the mirrors where the curvature can be made favorable (see Sections 3, 6.1, and 6.2 below).

A large number of kinetic instabilities, besides MHD perturbations, are likely to develop in the plasma due to the nonequilibrium character of the particle distribution function. Let us briefly consider some of them. Historically, the first one to discuss was the Dory–Guest–Harris instability [9] related to the perturbed drift of ions and electrons in the wave field. The ion drift velocity depends on the electric field averaged over the Larmor orbit and equaling $E_{\mathrm{eff}} = E_0 J_0(k_\perp \rho_\mathrm{i})$, where E_0 and $k_\perp$ are the field amplitude and the wave vector, respectively, J_0 is the Bessel function, and ρ_1 is the ion Larmor radius. The mean field for electrons practically coincides with the field at the point occupied by the particle. The dependence of the ion drift velocity on the transverse component of the wave vector explains why ions drift, within a certain range $J_0(k_\perp \rho_\mathrm{i}) < 0$, in the direction opposite to the drift of electrons; this discrepancy is responsible for instability. The Dory–Guest–Harris instability is greatly suppressed by the thermal spreading of particle velocities and is therefore difficult to observe in experiment.

The authors of Refs [10, 11] examined high-frequency (HF) convective instability developing due to plasma anisotropy that appears in the presence of a loss cone. To enable a wave excited by the developing instability to change the ion magnetic moment and effect ions escaping from the trap, its frequency must be higher than cyclotron frequency. For lower-frequency waves, the perturbation is adiabatic and does not lead to a change in the magnetic moment. In other words, the frequency of unstable oscillations must satisfy the inequality $\omega \geqslant \omega_{\mathrm{ci}}$, where ω_{ci} is the ion cyclotron frequency, and their phase velocity must fall into the region with a positive derivative of the transverse velocity distribution function, i.e., $\omega/k_\perp \approx v_\mathrm{i}$. These relations are held true if the oscillation wavelength is smaller than the ion Larmor radius: $k_\perp \rho_\mathrm{i} > 1$.

HF loss cone instability results from the buildup of magnetized oblique Langmuir oscillations satisfying the dispersion relation $\omega = \omega_{\mathrm{pe}} k_z/k$, where ω_{pe} is the plasma frequency of electrons, and having the phase velocity on the positive slope of the ion distribution function over transverse velocities and the frequency close to the ion cyclotron frequency. The growing oscillations have a high longitudinal group velocity; they are carried away from the trap before being fully developed, if its length L satisfies the inequality

$$L \leqslant 200 \rho_\mathrm{i} \sqrt{1 + \frac{\omega_{\mathrm{ce}}^2}{\omega_{\mathrm{pe}}^2}} ,$$

where ω_{ce} is the electron cyclotron frequency. More dangerous is drift-loss cone instability described in Ref. [11]; it can be regarded as absolute, since the excitable oscillations have the zero longitudinal group velocity. The development of this instability is associated with the buildup of electron drift oscillations interacting with ions featuring a nonmonotone ($\partial f/\partial v_\perp^2 > 0$) distribution over transverse velocities. The instability fails to develop if the plasma lateral size a defined by the density gradient

$$a = \frac{1}{\chi} = \left(\frac{1}{n} \frac{\mathrm{d}n}{\mathrm{d}r}\right)^{-1}$$

is not too small:

$$\chi \rho_\mathrm{i} \leqslant 0.38 \left(\frac{m_\mathrm{e}}{m_\mathrm{i}} + \frac{\omega_{\mathrm{ci}}^2}{\omega_{\mathrm{pi}}^2}\right)^{2/3} ,$$

where ω_{pi} is the plasma ion frequency. For a sufficiently dense plasma, this criterion is fulfilled, if the plasma radius exceeds $3-5\rho_\mathrm{i}$. It is worthwhile to note that both drift-loss cone and HF loss cone instabilities are highly sensitive to additions of small amounts of isotropic cold ions that strongly influence the derivative of the transverse-velocity distribution function at $v_\perp \approx 0$ [12]. The number of cold ions needed to stabilize drift-loss cone instability was calculated in Refs [13, 14]. The development of this instability in experiment and its suppression by the addition of a small number of cold ions were thoroughly studied by the M S Ioffe group at the National Research Centre 'Kurchatov Institute' and at the Livermore Laboratory using 2X and 2XIIB facilities [15].

Instabilities insensitive to fine details of the ion velocity distribution function are especially dangerous. One of them is Alfvén anisotropic instability [16–18] developing by the mechanism that involves the onset of resonance between longitudinal Alfvén waves and transverse movements of ions. Instability develops in the high-pressure plasma, if transverse and longitudinal ion temperatures are very different: $\beta_\perp (T_\perp/T_\parallel)^2 \geqslant 8$ [19], where $\beta_\perp$ is the ratio of transverse plasma pressure to magnetic field pressure. Such instability was observed, in particular, with the TMX (Tandem Mirror eXperiment) ambipolar trap [20] and in the GAMMA-10 [21] tandem mirror. TMX experiments gave evidence that a decrease in anisotropy of ions generated by the oblique injection of neutral beams into the trap with their subsequent charge exchanging and ionization in the plasma results in a reduced growth rate of Alfvén anisotropic instability [16].

By now the mechanisms of stabilization of plasma kinetic instabilities in open-ended magnetic traps have been fairly well explored both theoretically and experimentally. Nonetheless, the central problem of open systems even for the classical scattering rate — that is, the unacceptably high longitudinal plasma loss rate, remains fixed. Its solution required altogether new ideas for the creation of modified open plasma confinement systems with improved longitudinal confinement, such as ambipolar [22], multiple-mirror [22], and gas dynamic [8] traps. Ongoing ambipolar plasma confinement studies are comprehensively considered in review [24]. A detailed survey of research with 'classical' open magnetic plasma trap machines (probkotrons) is presented in Ref. [6]. The objective of the present work is to analyze results obtained in studies of GDTs. The reader is also referred to the excellent review article [25] for gaining additional information on magnetic mirror trap physics.

2. The gas dynamic trap (GDT)

2.1 Layout

The gas dynamic trap, a magnetic mirror version proposed by V V Mirnov and D D Ryutov in the late 1970s [8], is essentially a long axisymmetric solenoid with magnetic mirrors at both ends for plasma confinement (Fig. 3).

The mirror ratio is taken to be high, and the plasma in a solenoid is assumed dense enough, so that the ion mean free path for scattering into the loss cone becomes shorter than the trap length. The collisional plasma confined in the GDT central solenoid exhibits isotropic and Maxwellian velocity distributions of particles, save a small region in the immediate proximity to the magnetic mirrors. Such a design precludes the development of kinetic instabilities inherent in classical open magnetic plasma trap machines considered in preceding paragraphs.

The longitudinal plasma loss rate through the mirrors in GDTs is easy to estimate by multiplying plasma density, the plasma outflow rate roughly equal to the speed of sound, and the plasma cross section in the mirror. The resulting expression for the plasma loss rate assumes the form $nV_s\pi a^2/R$, where n is the plasma density, V_s is the ion-acoustic velocity, a is the plasma radius in the solenoid, and R is the mirror ratio. The value thus obtained does not depend on the collision frequency and is the upper estimate of the longitudinal loss rate. This parameter remains unaltered even if fast instabilities increasing the ion angular scattering rate develop. The plasma lifetime with respect to its outflow through the magnetic mirrors can be easily calculated by dividing the total number of particles in the solenoid, $n\pi a^2 L$, by the longitudinal loss rate, yielding

$$\tau_{gd} \sim \frac{n\pi a^2 L}{nV_s(\pi a^2/R)} = \frac{RL}{V_s} .$$

Evidently, the plasma lifetime in a GDT, in contrast to that in a conventional mirror trap, rather rapidly (linearly) increases with increasing mirror ratio. This observation permits us to obtain, by increasing the central solenoid length and the mirror ratio, lifetimes acceptable, in particular, for reactors [5]. The estimated lifetime may be used to specify requirements for plasma characteristics in the trap. Specifically, to have the loss cone filled, it is necessary that the gas dynamic confinement time exceed the one given by Eqn (1), i.e., be longer than the confinement time with an empty loss cone.

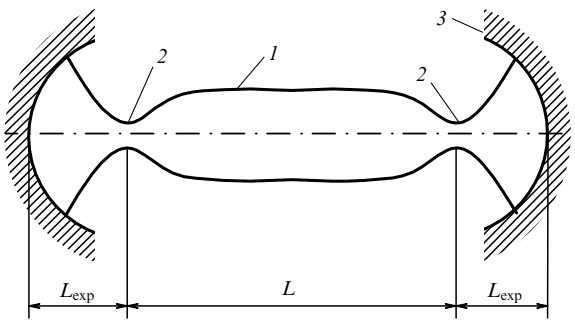

Figure 3. Schematic of a GDT device: *1* — magnetic field lines in the central solenoid, *2* — magnetic mirrors, *3* — end wall serving as a plasma absorber.

The plasma parameters must then satisfy the condition $RL/V_i \gg \tau_{ii} \ln R$ or $L \gg \lambda_{ii} \ln R/R$ [5, 8], where $\lambda_{ii} = V_i\tau_{ii}$ is the ion mean free path of scattering.

An attractive feature of GDTs is the possibility of stabilizing fast flute perturbations even in a magnetic system having axisymmetric geometry. To stabilize transversely small-scale modes, the Rosenbluth–Longmire criterion (2) needs to be satisfied. In the paraxial approximation (i.e., when slope angles of magnetic field lines to the axis are rather small) fairly well fulfilled for GDTs, the curvature is $\kappa \approx d^2r/dl^2$, where r is the field line radius, and l is the longitudinal coordinate counted along the line. In this approximation, it is convenient to use for the purpose of estimation an expression $\kappa \approx r/l_m^2$ relating the field line curvature to the characteristic length l_m of the field change.

Integral (2) has a negative value inside the long central solenoid with magnetic mirrors at both ends. Stabilization is attainable if plasma pressure behind the mirrors is high enough and the field line curvature is favorable for stability. In a simple probkotron, plasma density behind the mirror is vanishingly low. It can be estimated by equating collisional losses $N/\tau_{ii} \approx (RSL/\tau_{ii})\, n_0$ (here, N is the total number of particles in the trap, S is the plasma cross section area in the mirror, and L is the mirror-to-mirror distance) with the particle flux $Sn v_{Ti}$ in the magnetic mirror, where n is the plasma density behind the mirror. Considering the mirror ratio as being not too large, one obtains with a desired accuracy that $n/n_0 \sim \tau_{tr}/\tau_{ii} \gg 1$, where τ_{tr} is the characteristic time of ion flight through the trap. The longitudinal plasma loss rate in GDTs is much higher, so that the plasma density behind the mirrors is commensurate with that in the trap center. The rough stability criterion can be derived from the Rosenbluth–Longmire criterion (2) on the assumption that the effective value $\beta^{eff} = (p_{||} + p_\perp + \rho V^2)/B^2$ remains constant in both the central solenoid and the expander. Then, the stability criterion in the paraxial approximation takes the following form $\beta_c^{eff}/L < \beta_{exp}^{eff}/L_{exp}$, where the superscripts 'c' and 'exp' refer to the central part of the trap and the expander, respectively. To fulfill this criterion, the field in the expander must sharply weaken from the magnetic mirror toward the end wall, while the field lines have a greater favorable curvature corresponding to the small expander length L_{exp}.

The axial symmetry of the trap magnetic field is in itself an important technical advantage of GDTs and, moreover, excludes manifestations of 'neoclassical' transverse transfer mechanisms related to the nonnested character of ion drift envelopes [26]. It was shown in ambipolar trap experiments that these effects can be responsible for a significant rise in transverse losses (see, for instance, review [24]).

2.2 GDT-based neutron source

Prospects for the construction of a GDT-based fusion reactor are currently unclear. The effectiveness of such the reactor would highly depend on the characteristics of a magnetic field in the mirrors. The possibility of creating a magnetic mirror system with combined windings (warm and superconducting) was considered in Ref. [27]; the use of a purely superconductive winding was also discussed. It was assessed that the length of a reactor with a 45 T mirror magnetic field (i.e., that has already been closely attained with modern technologies for generating strong stationary magnetic fields) must be about 3 km with the power gain coefficient $Q = 3$ and the neutral beam injection power of 5 GW [5]. These estimates

seem implausibly high, but it should be remembered that the field in the main volume of a reactor does not exceed 1–1.5 T and is generated by simple axisymmetric coils. Further progress in warm superconductor technology would make it possible to generate a 40–50 T magnetic field in the mirrors by using purely superconductive windings and thereby considerably increase the competitive performance of GDT-based reactors. Moreover, the length of the trap can be reduced substantially (to ~ 1 km) by making its design slightly more sophisticated (e.g., instaling additional mirrors at both ends to reduce longitudinal plasma loss) [5, 28].

An important potential application of GDTs could be the creation of a 14-MeV source of neutrons produced in the D–T reaction. The analysis made in Ref. [5] demonstrated that such a neutron generator might possess unique characteristics even at plasma parameters close to those already achieved in open traps and, what is of a paramount importance, despite a rather conservative estimation of the prospects for their further improvement. Moreover, the generator can be created based on currently available technologies to exemplify the first practical peaceful application of a thermonuclear device. An important advantage of the GDT-based generator is the possibility of reaching the values of $\beta \sim 1$. The fusion reaction rate per unit volume is proportional to $n^2 \propto \beta^2 B^4$, which provides a basis for designing a relatively compact machine with a low power and tritium consumption.

The necessity of creating such a neutron source for the purpose of accelerated testing of materials and component units for a future tokamak fusion reactor plant is universally recognized. Its use would be instrumental in addressing such difficult physicotechnical problems as creating radiation-resistant engineering materials and those with low induced activity. The GDT-based generator has ample prospects for application not only in basic research in solid state physics and thermonuclear materials science but also as a device for afterburning the radioactive waste and radionuclide production or a hybrid nuclear power plant with a high degree of internal safety.

The most suitable device to serve as a neutron source is a GDT with a multicomponent plasma [5] consisting of relatively cold ($T_e \sim 1$ keV) and dense ($n \sim 10^{20}$ m^{-3}) plasma confined in the gas dynamic regime and a population of fast anisotropic ions undergoing longitudinal oscillations between reflection points near magnetic mirrors. Fast ions are generated by injection of deuterium and tritium neutral beams with an energy of ~ 100 keV and an angular spread of $\sim 1^\circ$ into the trap at a small angle ($\sim 20^\circ - 30^\circ$) to its axis. Due to the relatively low temperature of the target plasma, fast ions are slowing down efficiently than they are scattered. As a result, the ion angular distribution during the slow-down process remains almost as narrow as at its beginning. The longitudinal velocity of ions near turning points is low and they occupy this region for most of the period of longitudinal oscillations, which accounts for the higher density of fast ions here than in the trap center. The flux of neutrons formed in collisions between fast tritons and deuterons in this region can reach several MW m^{-2}, corresponding to the conditions under which the first wall of the tokamak reactor operates. Such a neutron source is needed to develop materials with prolonged lifetimes corresponding to the fluence of at least 10–15 MW year m^{-2} or ~ 100 displacements per atom in the lattice and with a minimum activation under the effect of neutron bombardment.

Table 1. Parameters of the neutron source [29].

Parameter	Variant				
	1	2	3	4	5
T_e, keV	1.1	1.00	1.00	1.00	2.00
T_i, keV	0.25	0.88	0.56	0.99	3.71
n_e, 10^{14} cm^{-3}	2.6	1.62	1.16	1.23	2.5
Injection energy, keV:					
Deuterium	69	100	100	100	50
Tritium	80	100	100	100	90
Plasma radius, cm	7.6	10.7	8.0	8.0	8.0
Mirror ratio R	11.3	15.0	15.0	23.7	17.0
Mirror magnetic field, T	17.5	18.0	18.0	28.0	28.0
Neutron flux, MW m^{-2}	2.1	1.3	0.63	2.1	3.3
Injection power, MW	48.00	59.6	79.3	57.5	43.8
Total power, MW	60.00	77.2	95.7	109.0	97.4

The calculated parameters of different variants of GDT-based neutron sources borrowed from Ref. [29] are presented in Table 1.

The marked enhancement of the critical field in superconducting systems [30] reached in recent years makes it possible to generate a desired field in the mirrors using no combined magnets with 'warm' coils. Practically all the power is then consumed in neutral beam injectors. It was calculated that an injection power of 60 MW and an injection energy of 65 keV are sufficient to ensure the desired neutron flux density in the testing zone (1–2 MW m^{-2}) at an electron temperature of 0.65 keV [31]. The GDT-based neutron source is shown schematically in Fig. 4.

A specific feature of this source is the relatively small neutron flux incident on the first wall, excluding the rather narrow zones intended for testing materials. Such a design makes unnecessary a frequent replacement of equipment in contact with the plasma in other regions. It should be emphasized once again that the longitudinal plasma loss rate in GDTs is defined by the majorizing estimate unrelated to the particle scattering rate. In particular, it is not suggested to reduce end losses by an electrostatic confinement as in

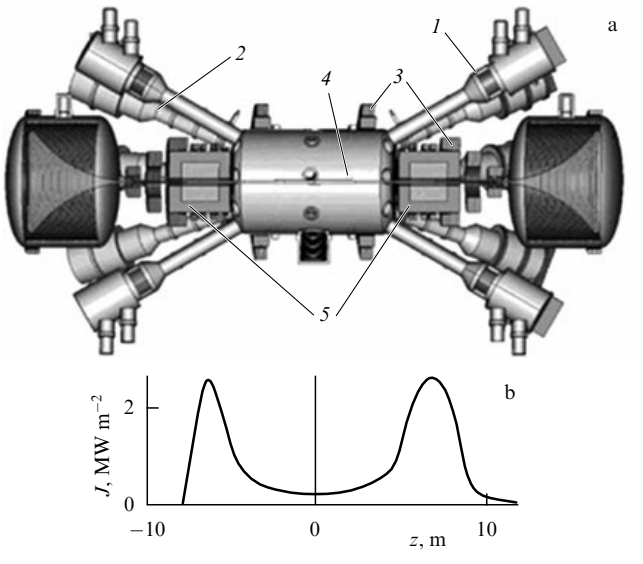

Figure 4. GDT-based neutron source: the layout (a) and 14-MeV neutron flux density (b). *1* — atomic beam injectors, *2* — beam dumps, *3* — magnetic coils, *4* — plasma, and *5* — testing zones.

tandem magnetic mirrors [22, 32] or based on the complicated and experimentally not proven thermal barrier concept [33]. At the same time, experiments have demonstrated the important role played in plasma confinement by ambipolar potential peaks arising at the fast ion turning points where their density is especially high (see Section 4).

Thermal ions in GDTs are retained in the collisional regime, and their density is high enough to ensure stability of fast injected ions with an anisotropic distribution function with respect to MHD perturbations and kinetic instabilities [12]. Moreover, it is known that the oblique injection of ions also improves their stability [16]. In a preceding section, we discussed the MHD stabilization mechanism involving plasma outflow into the region behind magnetic mirrors with a curvature of magnetic field lines favorable for stability. A few more methods for MHD plasma stabilization in GDTs have been proposed and explored experimentally. Reference [34] describes an end stabilizer (cusp) designed for additional electron cyclotron resonance (ECR) heating to enhance plasma stability. D D Ryutov and G I Stupakov [35] proposed using a nonparaxial probkotron in which stabilization occurs by virtue of plasma compressibility. References [36, 37] describe a magnetic divertor in the central part for stabilizing the plasma boundary by rapidly drifting particles retained in the region close to zero point of a field, while the authors of Refs [38–40] proposed placing a kinetic stabilizer behind the mirror. Ion injection into one end of the device was expected to be instrumental in creating and sustaining high-density plasma bunches in the regions with a favorable curvature of magnetic field lines in the kinetic stabilizer. End wall stabilization was also considered [41] on the assumption that the suppression of high-order flute instability modes will be possible due to effects of the finite ion Larmor radius and that the remaining solid-state displacement mode with a relatively small growth rate can be suppressed by a feedback method [42, 43].

Yet another specific feature of the axisymmetric magnetic configurations is small radial transport upon reaching MHD-stable regimes. Inherent in the GDT design are also two factors responsible for higher stability of the plasma with respect to microinstabilities. To begin with, neutral beams are injected at an acute angle to the magnetic field for improving plasma stability. In this case, the angular distribution of fast ions near the turning point is wide enough to reduce distribution anisotropy. Second, GDT design envisages the presence of a dense warm plasma showing isotropic Maxwellian distribution over velocities. The main parameters of various modifications of the GDT-based neutron source (GDT-NS) are collected in Table 2. The electron temperature is limited to $10^{-2}E_{\rm inj}$, where $E_{\rm inj}$ is the injection energy. This limitation does not follow from theoretical predictions; it is derived from the available database built up in the course of experimental studies and used for purely practical considerations. To recall, the value of $T_{\rm e} \approx 5 \times 10^{-2}E_{\rm inj}$ has been obtained in recent GDT experiments [44, 45] with additional ECR heating of electrons.

Longitudinal losses of the electron energy in GDTs are suppressed by a high degree of a magnetic field expansion from the mirror toward the end wall [46]. As a result, electron temperature depends on ion retention and is much higher than that predicted according to classical electron thermal conductivity on the end wall. As the length of the GDT-NS is increased and longitudinal losses additionally suppressed, the device can be regarded as the driver of the fusion–fission

Table 2. Parameters of a GDT-based neutron source [31].

	Beam/plasma	Beam/beam	Totally superconducting variety
Tritium beam energy, keV	240	94	65
Deuterium beam energy, keV	—	80	65
Tritium beam power, MW	20	6.5	20
Deuterium beam power, MW	—	8.5	20
Electron temperature, keV	0.6	1.1	0.65
Plasma density, m^{-3}	2×10^{20}	2×10^{20}	2×10^{20}
Plasma radius, m	0.06	0.08	0.06
Mirror ratio	20	15	10
Central field, T	1.25	1.8	1.3
Injection angle, degrees	20	40	30
Maximum neutron flux, MW m^{-2}	3.9	1.8	1.8
Consumed power, MW	50	60	47

system. The potential of the 14-MeV GDT-based neutron source used as the driver-afterburner of minor actinides (MAs) was evaluated in Ref. [47]. The basic GDT-NS model can be employed to carry out materials science research on the irradiation of materials for future fusion power plants.

It is worthwhile to note that the basic variety of GDT-NS is significantly inferior to other hybrid afterburners of transuranium isotopes in terms of efficiency. At present, hybrid fission devices comprising a $\sim$ 1-GeV proton accelerator, neutron-producing target, and subcritical nuclear assembly are considered to be the most technically mature systems. It was estimated in Ref. [48] that the comparable effectiveness of minor actinide burning in plasma facilities can be achieved for the gain coefficient $Q > 0.1$. Such Q values are guaranteed attainable with tokamak-based neutron sources, as well as in GDT-NS systems by raising the electron temperature in the plasma to 1.5–3 keV. Realization of this approach requires further physical research. Moreover, the design of the GDT-NS provides an opportunity to increase its length, thus heightening the neutron production per unit time, and energy efficiency of the source [47].

Therefore, the physical aspects of GDT-NS construction and exploitation require further investigation. They include demonstrating the rather high electron temperature and the stationary plasma confinement regime, the evaluation of plasma stability at high β, the influence of ambipolar potentials and plasma rotation on confinement, radial transport studies, etc. Moreover, the efficiency of various MHD stabilizers at appropriate plasma temperatures and densities needs to be estimated along with the possibility of using additional means of plasma heating, viz. ion cyclotron resonance (ICR), ECR, and axial injection of electron beams.

As far as engineering aspects are concerned, it is opportune to note that designing a GDT-NS is facilitated by the absence of axial plasma currents, which makes it possible to reach high β values in a stationary regime that excludes internal disruptions inherent in tokamak plasma. The design of used axisymmetric magnetic coils is based on currently available technologies, although further progress in engineering superconductive coils could greatly contribute to the improvement of GDT-NS characteristics (see above). Moreover, the following problems have yet to be resolved: the formation of continuous focused low-divergence neutral beams with an energy of 65 keV or higher and a power of 40 MW (their prototypes have already been produced [49] and further studies are underway [50–54]), the reception of a

plasma flux leaving the trap through the magnetic mirrors with a characteristic flow rate of 10^{22} particles s^{-1}, screening the sensitive elements from neutrons, creating a pellet injector with a frequency on the order of 1 kHz to maintain particle balance, etc.

Problems pertinent to the protection of GDT-NS equipment sensitive to neutron exposure were considered in Ref. [55]. The starting model was that of 'unoptimized rough' shielding in which the entire space between the plasma and the coils was protected, save sites only intended for neutral beam injection. In this way, the influence of the neutron flux on irradiation-sensitive components was reduced to a possible minimum. The critical level of neutron irradiation was determined for selected elements of neutral beam sources. This problem can be resolved, however, by means of local shielding. In a magnetic system, the coils located in the immediate proximity to injection ducts are exposed to especially strong neutron fluxes. The central coil experiences the strongest effect of the neutron flux, but its efficient local shielding extends the time during which the critical displacement per atom (DPA) is reached to longer than the 10-year period of GDT-NS operation. Although these results have been obtained under unoptimized positioning of shielding elements, they give reason to conclude that the GDT-NS concept is viable at the present stage of its development.

The application of GDT-NS to materials science research implies homogeneous irradiation of the entire specimen. Bearing in mind large gradients in the testing zones, this problem is addressed by using miniaturized specimens [56]. The active development of this approach is currently underway with special emphasis on the search for suitable samples and adequate testing methods [57, 58]. The GDT-NS project makes use of the tubular test assembly (TTA), allowing various materials to be irradiated, the specimen temperature to be changed and controlled, and each specimen to be treated on an individual basis. The design of the TTA should meet safety, reliability, and reparability criteria developed earlier for the International Fusion Materials Irradiation Facility (IFMIF) project [59]. Helium was chosen as a cooling agent by virtue of its safety, perfect compatibility with engineering materials at elevated temperatures, resistance to activation, and suitability for remote handling. The proposed design of the TTA with helium cooling is a hollow cylinder having ten irradiation chambers, each 2 m in length. Seven or eight chambers contain capsules with specimens at a given temperature, and the remaining two or three are intended for tritium reproduction examination.

Figure 5 depicts the TTA cross section with a plasma volume surrounded by a coolant (helium) and the outer wall. The interior of the TTA is designed in full conformity with the technologies developed for the IFMIF [58–60]. The irradiation chambers are arranged outside the vacuum vessel to ensure access to the specimens without decompression of plasma-containing part of the neutron source. The desired specimen temperature is maintained by an array of helium-filled pipes between the specimens and the capsules and between the capsules and the chamber walls, as in research reactors. Local ohmic heating systems can be used to improve temperature control of individual samples in TTA. Although all the capsules with specimens have identical geometries, but the size of the specimens in them can vary. Each chamber for tritium reproduction performance tests contains a few capsules with a lithium ceramic material. Tritium released by the specimens is swept up by helium gas flowing through the capsules; then, part of the coolant can be carried through thin pipes to the measuring equipment positioned near the neutron source. The fully-assembled TTA with a test volume of around 20 l housing up to 8000 specimens is displayed in Fig. 6.

The neutron dynamics in the GDT-NS TTA were simulated using the Monte Carlo N-Particle (MCNP) transport code. The test assembly was surrounded in the radial direction by a 12-cm-thick stainless steel liner and had a 28-cm thick neutron shielding (volume ratio of tungsten amounts to 90%, of water to 10%). Calculations were made taking into account the history of roughly 7×10^6 primary neutrons; due to this, statistical errors for all quantities were well below 1%. The profiles of neutron fluxes, DPA, and gas production rates in the TTA were obtained. The maximum irradiation dose was equivalent to15 DPA for a full year of operation, and did not drop below 10 DPA/year in most of the TTA volume, which was sufficient to test materials. The irradiation dose varied by 15% cm^{-1} in the radial direction, and by 0.5% cm^{-1} along the system's axis. The gradients obtained did not exceed 20% cm^{-1}, which restricted dose set inhomogeneity for materials science research [61, 56].

In the course of research carried out in Russia and the USA [62], several variants of the 14-MeV GDT-NS were proposed. In the concept under consideration, the physical

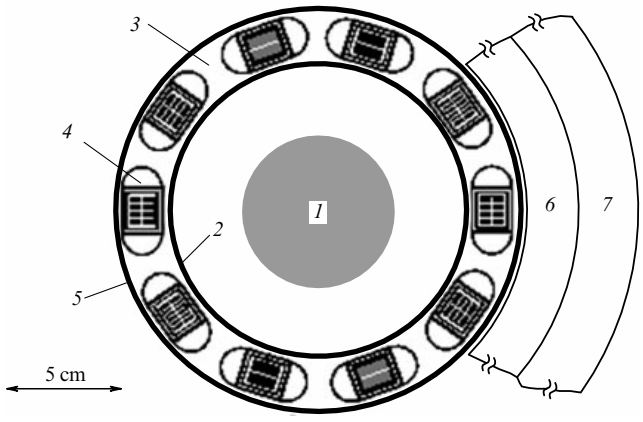

Figure 5. Schematic TTA cross section: *1* — plasma, *2* — inner wall, *3* — coolant (He), *4* — irradiated samples, *5* — outer wall, *6* — neutron reflector, *7* — neutron shielding.

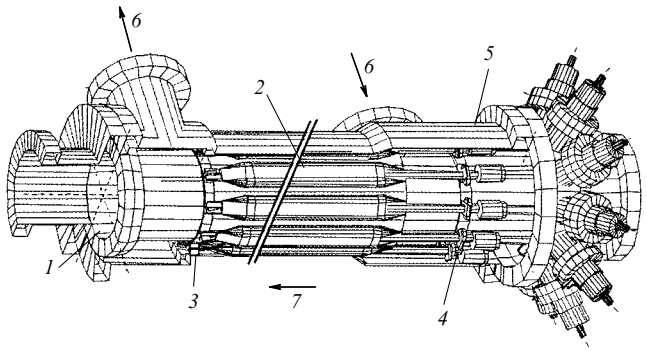

Figure 6. Testing zone of a neutron source: *1* — inner wall, *2* — chamber with specimens, *3*, *4* — mounting plates, *5* — outer wall, *6* — direction of a coolant flow, and *7* — direction toward the center.

dimensions of the GDT are similar to those of the existing facility, but the magnetic fields and neutral beam injection energies are four times higher. The power consumption is around 40 MW and depends on the desired electron temperature. Calculations reported in Ref. [63] suggest an approximate electron temperature dependence of 14-MeV neutron flux density on the wall:

$$\frac{P}{A}\left[\mathrm{MW\,m^{-2}}\right] = 2.5T_{\mathrm{e}}\ [\mathrm{keV}]\,.$$

Here, P is the power, and A is the area.

This equation holds true in the injection energy range from 65 to 105 keV. To recall, the calculated neutron flux density amounts to 0.5 MW m^{-2} at 200 eV (the electron temperature already achieved in GDT experiments with neutral beam injection [64]); it is comparable to neutron flux density in the ITER tokamak. Tokamak-based neutron sources for materials science have a 100-fold greater volume for the specimen arrangement than the GDT-NS, but depend on the production of tritium which quickly 'burns out' in the plasma. A comparison with accelerator-based sources shows that they have specimen arrangement volume that is 1% the size, and neutron spectra markedly different from those in reactors.

Turning back to GDT-NS, it should be mentioned that the main problems awaiting solution include the dependence of longitudinal electron energy losses on electron temperature and other parameters, as well as stability limits with respect to MHD and plasma microfluctuations in axisymmetric systems. A theoretical analysis of these issues yields an optimistic prognosis that, however, needs to be verified in experiment. The key technical problems address the formation of continuous neutral beams, development of technologies for tritium production and release, and creation of vacuum systems providing adequate pumping speed. These technological problems are common for all concepts of neutron sources based on magnetic confinement of D–T plasma.

One of the advantages of a GDT-NS is the relatively low consumption of tritium (around 150 g year^{-1}) combined with its small amount inside the device (less than 500 g). To simplify the system for reprocessing the pumped gas, atomic injectors are being developed to operate in a D–T mixture. In this case, the requirements for the degree of separation of deuterium and tritium are not very high, and cryogenic panels having different temperatures can be used for the purpose. The idea behind this approach was substantiated based on the results of experiments with a neutral beam of 40-keV energy, 1-MW power, and 1-s beam duration, conducted in Novosibirsk. The injector fed the D–H mixture directly into the beam source through a pulse valve. The relative deuterium concentration in the mixture varied from 0 to 100%. The measured parameters of the beam at optimal perveance proved to be in excellent agreement with the theoretical ones calculated with due regard for the beam's molecular composition [65].

It is worthwhile to note that applications of GDT-NSs can be additionally extended by modulating the neutron flux in a desired frequency. Modulation provides an efficient tool for evaluating the role of nonstationary effects in continuous-action fusion facilities and for the precision measurements of weak signals by the synchronous detection method in basic research. The authors of Ref. [66] demonstrated the possibility of modulation in a frequency up to 1 kHz and a depth of several percent; they also discussed limitations on the modulation amplitude at higher frequencies. One of the methods for modulation of a neutron flux by means of periodic injection of a neutral beam giving rise to short-lived density peaks near the turning point was considered in Ref. [67]. It is shown that the simultaneous appearance of deuterium and tritium peaks at the turning points may be responsible for periodic short neutron bursts with an intensity 1.5 times the mean level.

To conclude this section, the following advantages of the proposed GDT-based neutron source for materials science research should be emphasized:

- The natural continuous mode of operation of the neutron source. The possibility of modulating the neutron flux in a characteristic frequency of a few kilohertz. The availability of a comprehensive open-ended magnetic traps' database. The data necessary to realize the continuous operation regime of the generator can be obtained with the help of either a hydrogen prototype of the neutron source that does not need special shielding or with a specialized facility.
- The value of $\beta \sim 1$ can be reached in open-ended magnetic traps (i.e., plasma pressure can be close to the pressure of a confining magnetic field), allowing facilities to be created with large neutron fluxes and a plasma volume as small as several litres for testing materials.
- The possibility of creating a source with a 1–2-MW m^{-2} neutron flux and a large ($\sim$ 100 l) testing zone to form blankets for tritium production.
- Electron temperature can be raised to self-consistent values under conditions of suppressing cold secondary electron fluxes emitted from the end wall. The relevant theory proposed in Refs [68, 69] is confirmed in experiment [70]. A rise in electron temperature would allow the heating power to be decreased at a given neutron flux in the test zone.
- Low tritium consumption ($\leqslant$ 0.2 kg year^{-1}) with a small amount of this isotope in the facility. It does not need to be produced in the system and can be obtained from a commercial source. A tritium recovery system can be integrated into the facility if appropriate.
- High density of the neutron flux ($>$ 2 MW m^{-2}) permits accelerated testing of materials in a volume $\geqslant$ 1 l.
- The small neutron flux outside the test zone ($\leqslant$ 0.1 MW m^{-2}) and insignificant thermal load ($\leqslant$ 0.6 MW m^{-2}) there spares the facility from critical impacts.
- The primary D–T neutron spectrum corresponds to the first wall irradiation conditions in tokamak reactors. The spectrum has no tail of high-energy neutrons, as in accelerator-based spallation reaction [71] or stripping reaction (D–Li IFMIF type) [72] sources.
- The source makes use of simply designed and therefore inexpensive magnets.
- Well-developed positive ion-based neutral beams can be applied to heat and sustain plasma in the neutron source, as it enters the continuous working regime.
- Expansion of the plasma jet behind the mirror in the flaring magnetic field permits reducing thermal load on the plasma dump surface to an acceptable level of 1 MW m^{-2} or less.
- Only those technologies that have been developed specially for fusion research are employed to design, construct, and operate the facility, viz. neutral beams or possibly additional ECR- and ICR-heating, superconducting magnets, tritium systems for the neutron source operated in the continuous mode for $Q < 1$.
- The estimated construction cost of the neutron source is $\sim$ 10% of the ITER cost.

• The neutron source can be put into operation with a hydrogen plasma, which permits activation of engineering materials to be avoided at this stage.

Notice also that new approaches to the improvement of open-ended magnetic traps continue to be proposed, despite the long history of their development. By way of example, the employment of a helical type mirror is likely to facilitate longitudinal plasma confinement in a gas dynamic trap [73] or to increase the efficiency of a GDT-based plasma engine by reversing the direction of plasma rotation [74].

2.3 Experimental setup at the Budker Institute of Nuclear Physics, Novosibirsk

The work of V V Mirnov and D D Ryutov [8] provided a basis for the construction of a facility intended to verify basic premises of the GDT theory at the Budker Institute of Nuclear Physics, Siberian Branch of Russian Academy of Sciences (Novosibirsk). Despite its relative simplicity and small size, the results obtained in experiments are crucial for both basic plasma physics and solution of applied physics problems dealing with the creation of a neutron generator.

The GDT consists of a 7-m long central solenoid (Fig. 7), a vacuum chamber about 1 m in diameter in the central part, and two end expander tanks 2.6 m in diameter each. The total volume of the vacuum chamber is 15 m^3. The working pressure in the central part before a shot ranges $(0.5-1)\times 10^{-7}$ Torr. The magnetic field is generated by coils placed directly on the central vacuum chamber and by the mirror sections. The trap is preliminarily filled with plasma from a plasma gun mounted on one of the end tanks. Characteristic parameters of the plasma in the GDP are listed in Table 3.

The magnetic field profile in the expander is varied with the aid of coils mounted on the end tanks and fed from an independent power supply. The maximum value of the field generated by the source on the axis is around 200 Oe. If the coils are switched off, the magnetic field lines in the expander are practically straight, and their mean curvature is close to zero. By varying current in the reversed field coils, the curvature can be made either favorable (if current in the coil is opposite to that in the coils of the central solenoid) or unfavorable (if coils are connected consistently) for MHD stability. Moreover, a pair of closely spaced coils with oppositely directed currents inside one of the end tanks (left one in Fig. 7) can be used to form a cusp type magnetic configuration in the absence of a magnetic field on the axis.

Table 3. Parameters of a GDT device.

Parameter	Value
Mirror-to-mirror distance, m	7
Magnetic field in central cross section, T	Up to 0.35
Mirror magnetic field, T	2.5 – 15
Plasma density, m^{-3}	$(1-6)\times 10^{19}$
Plasma radius in central cross section, cm	6 – 7
Electron temperature, eV	Up to 250 (up to 10^3 with additional ECR heating)
Particle energy of hydrogen or deuterium beams, keV	20 – 25
Pulse duration, ms	5
Total injection power, MW	up to 5.4
Injection angle, degrees	45°
Fast ion density in stagnation region, m^{-3}	$\approx 5\times 10^{19}$
Mean energy of fast ions, keV	≈ 10
Maximum local β	0.6

The lifetime of the particles captured between the outlet axial and radial mirrors in the cusp is sufficiently long, unlike that in the expander with the field continuously decreasing toward the end wall; it is several times the time of flight. Due to this circumstance, the plasma flux from the central solenoid maintains a high enough particle density in the cusp, which, together with the large favorable curvature of the magnetic field lines, ensures a considerably greater favorable contribution to stability in the cusp than in the expander.

The magnetic mirrors of the trap are formed by external large-radius coils serially connected to the solenoid magnetic system and internal coils fed from an independent power supply. Such a design makes it possible to vary the field in the mirrors up to 16 T or the mirror ratio in the range from 12.5 to 100, while the central field varies from 0.1 to 0.35 T. Changes in the mirror field have practically no effect on the field strength and the curvature of field lines in the central solenoid and the expanders.

To reduce charge exchange losses of fast ions, it is needed to weaken neutral gas recirculation from the wall of the vacuum chamber. For this purpose, an array of electric arc titanium evaporators was placed inside the central cell of the GDT. Both the arrangement and the switch-on time of the evaporators were optimized, so as to ensure rapid and uniform coating of the wall surface before the next experiment. To improve adhesion of the titanium film, the inner surface of the chamber was covered with stainless steel panels that had preliminarily undergone a few stages of special

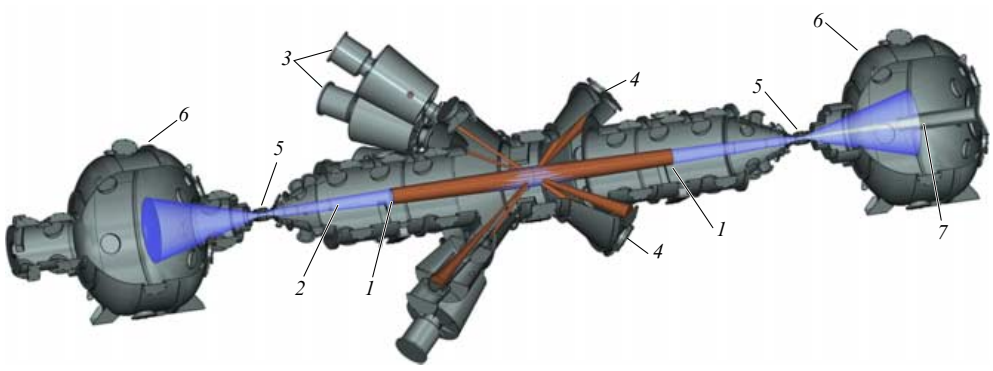

Figure 7. Experimental setup: *1* — stagnation points of fast ions, *2* — warm plasma, *3* — atomic beam injector, *4* — beam dump, *5* — mirror units, *6* — end tanks, and *7* — arc-discharge plasma source.

treatment, including a sandblast finish of their plasma-facing surfaces and vacuum thermal degassing near 800 °C. The system of evaporators made it possible to increase the mean lifetime of fast ions with respect to charge exchange from 1 to 10 ms, and to maintain pressure in the central cell during experiments at a level of $(0.5-1.1)\times 10^{-5}$ Pa. A detailed description of the vacuum system, including the set of titanium evaporators, the preliminary preparation procedure, and experiments on measuring the dynamics of the neutral gas in the GDT during injection of heating neutral beams, can be found in Ref. [75].

A variety of diagnostic techniques were applied to measure plasma characteristics in the GDT central cell [76]. The radial profile of plasma density was measured near the GDT central cross section by two methods: from heating beam attenuation or alternatively with the involvement of the Thomson scattering system. The temporal evolution of the radial plasma density profile was followed up with the employment of a diagnostic option based on the charge exchange of the deuterium atomic beam with an energy of 25 keV (the spatial and temporal resolutions of the method were 1.5–2.0 cm and 50 μs, respectively) [77]. The radial electron temperature profile was measured with the Thomson scattering system, and the time dependence of ion temperature was derived from Rutherford scattering of the diagnostic neutral beam [70–80]. It was revealed that ion and electron temperatures turned out to be very similar by the end of the heating beam injection pulse [81].

The radial profile of the magnetic field in the region where fast ions stopped was measured by the optical diagnostic technique based on the dynamic Stark effect [82–84]. For this purpose, a diagnostic neutral beam with small angular and energy spreads [85] was injected normally to the GDT axis. In this case, an electric field $\mathbf{E}=[\mathbf{vB}]/c$ responsible for the splitting of atomic energy levels appeared in the reference frame moving together with the beam. The degree of splitting was linearly dependent on the magnetic field value and its evaluation served as a reliable tool for local measurements of the magnetic field. The spatial resolution of this diagnostic technique — depending on the beam size and the visual angle of the receiving optics — was 4.5 cm along the observation chord, and 1.5 cm along the GDT axis. The radial profile of relative plasma pressure $\beta_{\rm v}=8\pi p/B_{\rm v}^2$ could be found from the results of measurements of the magnetic field in experiment (B) and of the vacuum magnetic field ($B_{\rm v}$); in the paraxial approximation, these quantities are related through the simple formula $\beta_{\rm v}\approx 1-B^2/B_{\rm v}^2$.

The trapped power of heating neutral beams was determined from beam attenuation measured by secondary emission detectors. The energy content of fast and warm plasma components was found based on diamagnetic loop measurements. The powers of charge exchange losses and plasma radiation were measured with the aid of a set of pyroelectric bolometers with a temporal resolution of 10 μs. Some of the fast ions underwent neutralization near the GDT central cross section due to charge exchange in the gas and escaped from the plasma within a rather small pitch-angle interval around the injection angle of 45°. A comparison of the data obtained using an open bolometer and one with a narrow collimating tube made it possible to distinguish between charge exchange losses of fast ions having a narrow angular interval and emission uniformly distributed over the entire solid angle. These diagnostic procedures are described in detail in Refs [75, 76]

Data about the local distribution function of fast ions were obtained from an analysis of atomic fluxes formed due to charge exchange on an artificial target [86, 87]. The target was a diagnostic hydrogen neutral beam with an energy of 13–15 keV, beam current up to 25 equivalent amperes, and pulse length of 120 μs [87]. Particles experiencing charge exchange in the artificial target passed through the stripping target as they left the plasma; they were separated in a 45-degree electrostatic analyzer and detected by microchannel plates. The shot-to-shot displacements of the analyzer to different distances along the GDT axis and variation of its angle of inclination made possible measurements of the angular distribution of fast ions within $45^\circ\pm 5^\circ$. The angular resolution of the analyzer varied in the $0.35^\circ-0.8^\circ$ range depending on its position, energy resolution changed from 0.4 to 1.3 keV when measuring the particles with energies from 2.8 to 20 keV, and spatial resolution was $8\times 6\times 2.5$ cm^3. The diagnostic hydrogen beam was utilized to measure effective ion slowing down time in the plasma and (in combination with a modified electrostatic analyzer) radial profiles of charge-exchanged atomic fluxes (see Section 4) [88].

Plasma parameters in one of the end expansion tanks housing no plasma gun were measured using the following set of diagnostic tools:

- movable emissive probe to measure plasma potential;
- movable grid probe to measure ion flux density;
- movable bolometer to measure energy flux density;
- electrostatic end loss analyzer to measure the ion energy distribution function, and
- retractable Langmuir probe to measure the mean electron energy and plasma potential.

The probes and the bolometer were installed on the movable segment of the end wall with an axial stroke of 120 cm, which allowed it to be placed directly in the mirror in the innermost position. In addition to the data coming from the set of probes, the plasma potential along the expander axis was measured by the local gas target method. The target was prepared by pulsed injection of working gas through a glass capillary placed in different positions along the expander axis. Cold ions resulting from charge exchange and ionization of the gas cloud were accelerated by the ambipolar potential and detected by an analyzer mounted on the end wall. The potential at the gas target point was deduced from the particle energy measured by the analyzer.

3. Magnetohydrodynamic stability of plasma without auxiliary heating when stabilized with an expander

An unfavorable contribution to the mean curvature (2) comes from the transition section inside the long GDT probkotron. In the case of an isotropic plasma and a high mirror ratio, when pressure inside the trap can be assumed constant, this contribution is minimal for the following shape of the magnetic field lines running through the transition section [5]:

$$r(l)=r_0\sqrt{1-\frac{R-1}{R}\,\frac{l}{l_{\rm m}}}. \tag{3}$$

Here, $l_{\rm m}$ is the length of the transition section, and l is the longitudinal coordinate counted from its origin.

Magnetic field lines of the GDT have a near-optimal shape. Their optimal shape in the presence of anisotropic injected ions is significantly different from the shape calcu-

lated from formula (3); under strong anisotropic conditions, a line of force sharply bends near the ion turning point [89, 90]. In this case, the mean curvature may become favorable for MHD stability.

Earlier experiments were designed to study the stability of the plasma produced by a plasma gun [91]. The gun was placed behind the magnetic mirror to operate for around 3 ms, during which plasma density in the center increased to $(5-7)\times 10^{19}$ m^{-3}. The electron temperature of such a gun-driven plasma was 3–10 eV. The radial density profile had a roughly Gaussian shape with a characteristic width along the radius of 6–7 cm that weakly depended on the magnetic field in the plasma gun location. The injection of neutral beams markedly broadened the plasma density profile.

As the plasma gun operated, the magnetic field lines were frozen into the end wall on which it was mounted [92], so the plasma behavior in the solenoid was not sensitive to the confining magnetic field geometry. The gas-discharge plasma had a high density and conductivity across the magnetic field, which prevented the formation of transverse electric fields in the plasma column through the development of flute perturbations. After the plasma gun was switched off, the plasma behavior depended on the magnetic field line curvature in the plasma expansion region behind the mirrors. This allowed studying the plasma stability boundary and the dependence of the azimuthal mode spectrum on the parameters of the plasma and the magnetic field. An interesting feature of GDTs is the capacity to change within a wide range the mean curvature of magnetic lines of force in the trap with an expander in the stabilization regime. In the experiments described below, different methods were utilized to make such changes, viz. (1) altering the mirror ratio, (2) additional ICR heating in the trap center, which yielded fast strongly anisotropic ions, (3) local alteration of the curvature in the central part by special coils, and (4) changing the curvature of magnetic field lines behind the mirrors.

Figure 8 plots time dependences of plasma line density during decay. If the magnetic field line curvature in the expander is unfavorable, the plasma experienced the action of strong instability and quickly left the trap (curves *1*, *2* in Fig. 8). In such a case, the Langmuir probes placed inside the trap 4.8 m apart along the same line of force detected well-correlated high-amplitude density perturbations. Determination of the perturbation structure along the azimuth by a set of probes in the trap and flux sensors in the expander revealed the predominance of the rigid-body displacement mode, $m = 1$, suggesting whole plasma column displacement across the confining magnetic field and the loss of plasma at the biased radial limiters. The characteristic time of plasma column displacement soon after switching off the plasma source ranged $\sim 50-100$ μs.

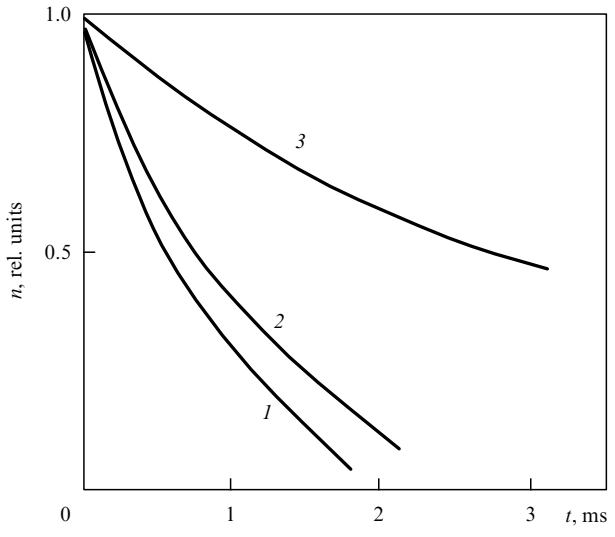

Figure 8. Behavior of plasma line density during decay: *1* and *2*— unfavorable field line curvature in the expander, *3*— favorable curvature. Time is counted from the time the plasma gun is switched off.

The length of the ion Larmor radius (which as a rule is much greater than that of electrons) greatly affects the flute mode growth rate. The drift motion of an ion in flute oscillations depends on the electric field averaged over its orbit and markedly differs from electron movements, if its Larmor radius is commensurate with the wavelength. The effect of the finite Larmor radius (FLR) [93] for $\rho_i l_m/a^2 \gg 1$, where a is the plasma radius, results in stabilization of all flute modes but $m = 1$, in which the perturbation field is uniform over the plasma column cross section, while drift velocities of ions and electrons coincide. For a longitudinally inhomogeneous plasma, FLR effects become significant for $\rho_i\langle l_m\rangle/a^2 \gg 1$, where the angle brackets denote averaging over the length of the trap with plasma weight β.

An important feature of the experimental GDT model is a possibility of widely varying the $\rho_i\langle l_m\rangle/a^2$ values. The weighted average length $\langle l_m\rangle$ of a change in the magnetic field can vary depending on the field line curvature in the expansion tanks and in the central part of the GDT; it also depends on the mirror ratio (as this takes place, the plasma density behind the mirrors also changes). In particular, if the contribution from the expanders counterbalanced the unfavorable contribution of the trap central section to the mean curvature of the magnetic field lines, it formally corresponded to $\langle l_m\rangle \to \infty$. Moreover, the mean Larmor radius could be altered by ion cyclotron heating in the central solenoid of a GDT. The opposite case of small $\langle l_m\rangle$ was realized by increasing the unfavorable contribution to the stability criterion determined by the central section of the trap. To this end, the optimal magnetic configuration of magnetic field lines was distorted by the introduction of an additional coil placed near the trap center, so that the lines of force had a greater positive curvature in the region of high plasma pressure. To recall, a change in both the mirror ratio and the shape of magnetic field lines in the central cell of the GDT altered the strength of the magnetic field in the expanders by less than 1% (and vice versa), greatly facilitating the interpretation of the data obtained. The contribution from the central solenoid could be varied, too, by setting the ion cyclotron resonance area in the trap center with the maximum field line curvature or near the mirrors. As noted above, the Larmor radius of ions increased in either case, but in the former one a localized population of high-pressure anisotropic fast ions formed in this region.

Figure 9 plots the dependence of the width of the unstable azimuthal harmonic spectrum on parameter $\rho_i\langle l_m\rangle/a^2$. Evidently, the spectrum is wide when the indicated parameter is small and narrows to mode with $m = 1$ when its value is large.

The influence (even if indirect) of the FLR effect on the unstable flute mode spectrum was also observed in experiments described in Ref. [94]. True, these data are difficult to compare with theoretical ones, because the authors did not

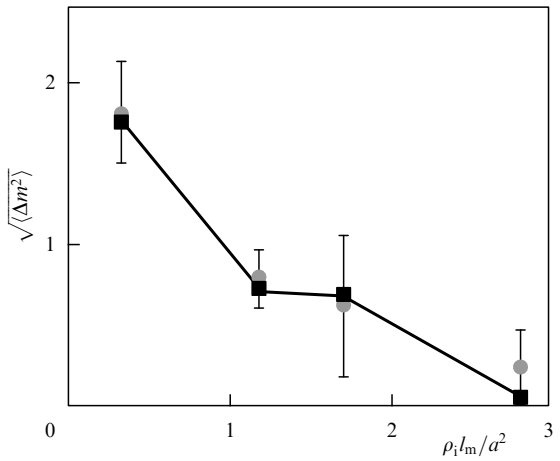

Figure 9. Width of the unstable harmonic spectrum versus parameter $\rho_i l_m / a^2$.

undertake quantitative impact evaluation. Nevertheless, the results of these experiments are in excellent agreement with the theoretical model of flute instability taking into consideration FLR effects within a wide range of plasma and magnetic field characteristics [95].

The dependence of the trap plasma lifetime variations in the range from 12.5 to 75 on the mirror ratio is shown in Fig. 10. On the whole, the expected linear dependence correctly describes the experimental data for $R \leqslant 35$. It was shown that the plasma lifetime begins to fall at higher mirror ratios due to development of flute oscillations, because the decreased plasma flux to the expanders reduces their favorable contribution to stability. Measurement of the temporal evolution of the radial plasma density profile for $R > 35$ gave evidence of developing large-scale MHD instability.

Analyzing these data permits us to conclude that the stabilizing contribution of the expanders under the standard operating regime of the facility at $R = 25$ is 1.5–2 times greater than the destabilizing contribution from trap central section. Introducing notation Δ_s for this quantity, which can be referred to as the plasma stability margin in the GDT, yields $\Delta_s = 1$ at the stability boundary. The value of Δ_s at the stability threshold corresponds to the length of change of the magnetic field, determined earlier as $\langle l_m \rangle \to \infty$. Results of the measurement of the plasma lifetime at a constant expander configuration depending on the calculated unfavorable contribution from the trap central section for different coil currents are presented in Fig. 11. They also indicate that the 'stability margin' at $R = 25$ is $\Delta_s = 1.5-2$.

The plasma lifetime under stable confinement conditions at a temperature of several electron-volts and density of $10^{19}-5\times10^{20}$ m^{-3} is in excellent agreement with that predicted by the gas dynamic model. The measured energy and particle fluxes are consistent with calculated results [29].

Notice that an increase in the average favorable magnetic field line curvature in the trap reduced plasma response to external perturbations, such as azimuthal inhomogeneities of heating and plasma replenishment, and to perturbations of the trap vacuum magnetic field, as was confirmed in special experiments [96].

The data on stability boundaries in GDTs presented in Figs 9–11 are in a reasonable quantitative agreement with the theory briefly reviewed in the Introduction [5, 8].

At the same time, a comparison of measured and predicted stability limits taking account of the plasma pressure spatial profile shows that its experimental value is much smaller than the theoretical one. The reason for the difference is not quite known. It is possibly related to the uncertainty in the choice of the maximum value of $\chi\rho_i$ at magnetic field lines in the expander, determining the upper limit in stability integral (2). A reduction in the limiting value of $\chi\rho_i$ from 0.5 to 0.3 in the calculations allows an acceptable agreement to be reached between theory and experiment. It cannot be ruled out, however, that the observed quantitative difference between measured and theoretical stability limits is due to the influence of certain undocumented phenomena in the GDT expander, such as finite resistance of end plasma damps [97]. Taking into account the finiteness of plasma conductivity may also exert an equally strong influence on the results of measurements, especially at low plasma temperatures [98]. To recall, the stabilizing contribution of expanders was calculated only in limiting cases of adiabatic and isothermal plasma flows in them [5]. At the same time, direct measurement of plasma flow parameters [99, 100] demon-

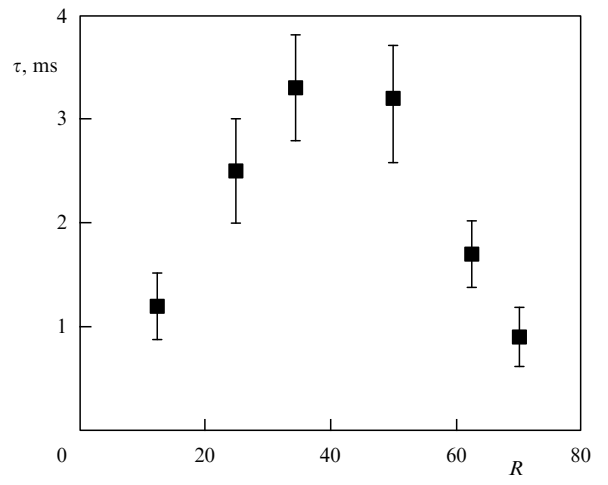

Figure 10. Trap plasma lifetime versus mirror ratio.

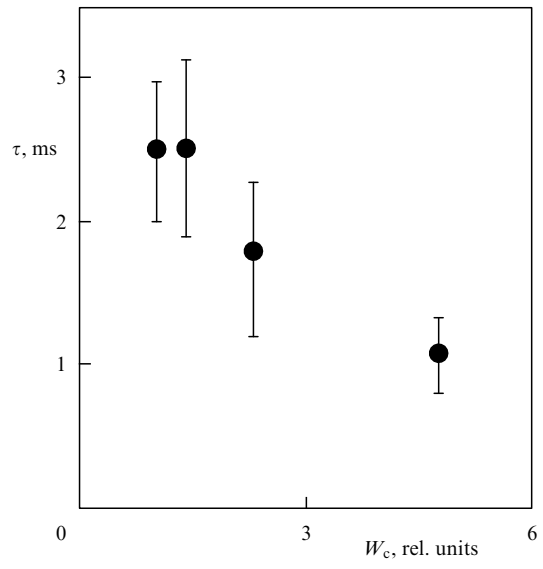

Figure 11. Plasma lifetime versus the unfavorable contribution from the GDT central section to the stability integral.

strated that they are significantly different from those in both regimes and come nearer to the values predicted for the adiabatic regime only in the case of additional plasma heating. Moreover, additional effects are likely to occur if the finite size of ion orbits, which is sometimes comparable with the radius of curvature of magnetic field lines in the expander, is taken into account. The finite β value of the plasma in the expander and the nonparaxiality of the magnetic field lines may also be responsible for the observed quantitative difference between experimental and theoretical stability limits. Similar difference was documented in ambipolar trap experiments [101, 102]. For example, Ref. [101] reports an almost 6-fold difference between the measured and calculated stability limits. A more detailed description of experiments on gun-driven plasma stability in GDTs can be found in Ref. [91]. Results of the measurement of MHD stability limits for heated plasma in GDTs are presented below.

4. Plasma heating by neutral beams and confinement of fast ions

To heat the warm initial plasma, hydrogen neutral (deuterium) beams were injected into the trap in the central plane of the solenoid at an angle of 45° to the axis. The injection power amounted to 4.3 MW at a particle energy of 15–17 keV. The duration of injection in the first experiments was 0.25 ms; thereafter, it was increased to 1.2 ms, then to 5 ms at a power in excess of 6 MW and an energy of 23–24 keV. Characteristics of heating neutral beams are listed in Table 4.

In experiments with a 1.2-ms duration of neutral beam injection, the plasma captured fast protons (deuterons) with a power up to 2.6 MW [103] as the result of partial ionization and charge exchange of beam particles. The injection gave rise to fast ions undergoing oscillations between reflection points near magnetic mirrors. Accumulation of these ions and their slowing down at the electrons increased the electron temperature to 100 eV at a primary plasma density of $(3-5)\times 10^{19}$ m^{-3}. Ion temperature in the primary plasma remained similar to the temperature of electrons in the absence of neutral beam injection. Measurement of plasma energy balance showed that the electron temperature is determined by the balance of power transferred to electrons from fast particles, leveling electron and ion temperatures in the primary plasma, and collisional losses in the magnetic mirrors.

A comparison of measured and theoretical characteristics of fast ions gives evidence that their slowing down and angular scattering in the plasma are governed by the mechanism of binary Coulomb collisions with an accuracy of 10–20%. Figure 12 presents, by way of example, measured and theoretical time dependences of fast ion energy content.

Table 4. Parameters of the neutral beam heating system.

Parameter	Value	Total value
Ion current, A	35 – 45	330
Beam energy, keV	23 – 24	
Ion beam power, MW	0.81 – 1.1	7.7
Angular divergence, mrad	18 – 21	
Ion neutralization efficiency in the target	0.85 – 0.86	
Beam track acceptance	0.73 – 0.95	
Neutral beam power at the plasma boundary, MW	0.51 – 0.83	around 5.4

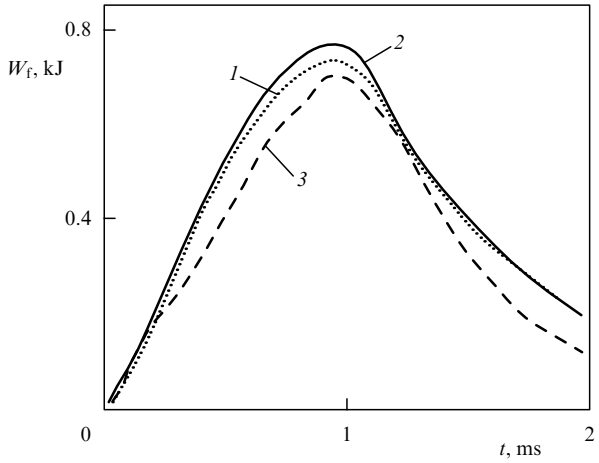

Figure 12. Time dependences of fast ion energy content: *1* and *2* — theoretical curves obtained using the Monte Carlo method and the Fokker–Planck equation, respectively, and *3* — experimental curve [104].

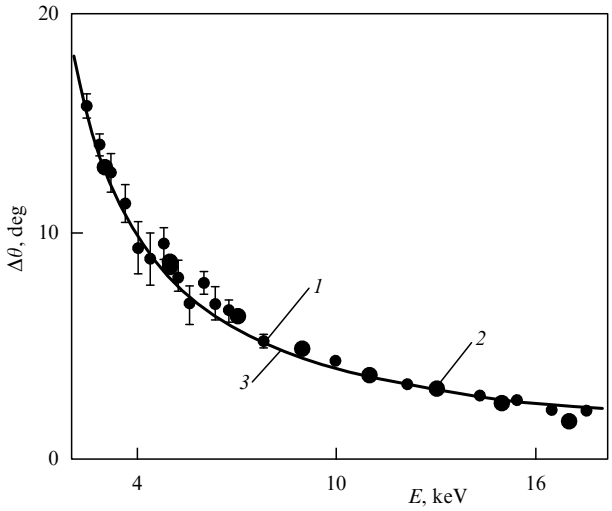

Figure 13. Energy dependence of fast ion angular spread 0.6–0.9 ms after the onset of atomic injection: *1* — experiment, *2* — Monte Carlo calculation, and *3* — model simulation.

The energy dependence of an ion angular spread is shown in Fig. 13. Measured temperatures and densities of the target plasma were used in calculations. The agreement between experimental and theoretical parameters of fast ions suggests the classical character of their interaction with the target plasma, which needs to be taken into consideration if the desired parameters are to be achieved in a GDT-based neutron source.

This conclusion was further confirmed by measuring the longitudinal profile of the fusion proton flux in the GDT solenoid, following injection of deuterium beams. The measurements were made with collimated detectors of fast (3.02-MeV) protons of the D–D reaction. The fast protons appeared in nearly half of deuterium fusion reactions; therefore, measurements of proton flux density unambiguously correspond to neutron flux density in the D–D reaction. Due to the narrow angular distribution of deuterons, the profile of the flux of thermonuclear reaction products must have peaks in the region of turning points for fast particles, as in the neutron source. The results of measurements are presented in Fig. 14 [104] with the distance counted from the

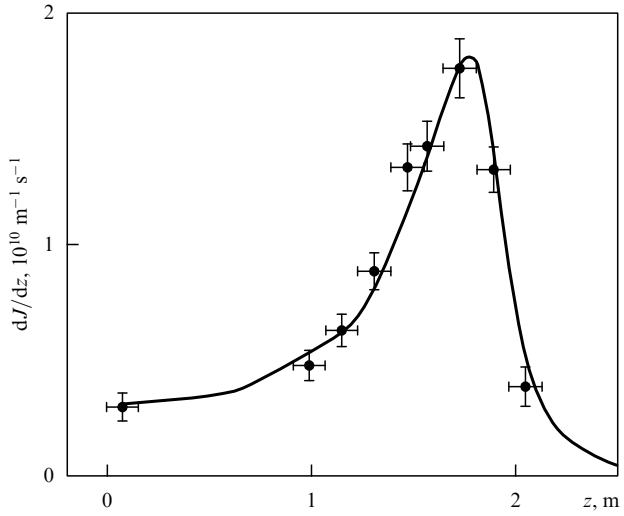

Figure 14. Longitudinal emission profile of fusion protons, measured with a collimated detector and calculated (continuous curve) [104].

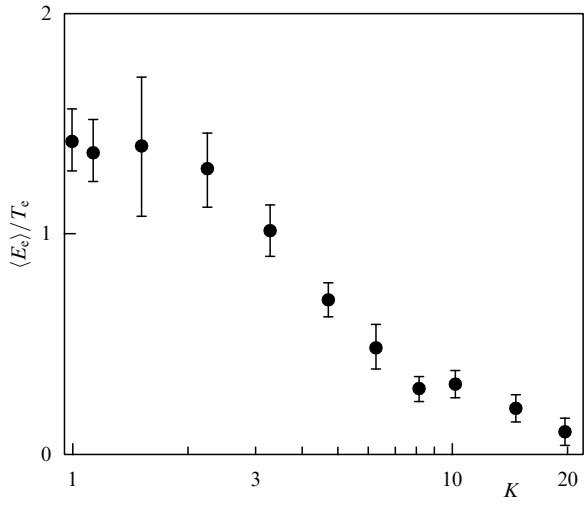

Figure 15. Mean electron energy in the expander depending on the expansion degree.

trap center toward the magnetic mirror. The reflection point for the ions having a pitch angle of 45° in the center corresponds to $z = 180$ cm.

The vicinity of the turning points for fast deuterons has a narrow radial profile with characteristic dimensions close to the Larmor radius of the particles with a mean energy of 8–9 keV. Ion density amounts to $\sim 5 \times 10^{19}$ m^{-3}, and the local value of $\beta \approx 0.6$ [64]. In other words, the possibility of confining plasma with a pressure comparable to that of the magnetic field in a GDT was confirmed in experiment.

5. Suppression of electron heat flux

The most serious challenge facing open-ended magnetic trap designers and researchers remains the too large heat losses in the plasma in contact with the end wall. Hot electrons arriving at the wall from a trap are replaced by cold secondary electrons which, in turn, go back to the trap. If, however, the magnetic field at the wall is lowered with respect to the mirror field by a factor of $\sqrt{m_i/m_e}$ or more, the situation changes dramatically. Let us denote magnetic fields on the wall and in the mirror by B_w and B_m, respectively. The density of ions traveling toward the wall drops because the total ion flux through the field line tube is constant. Once ion acceleration in the ambipolar potential jump behind the mirror is disregarded, ion density depending on actual magnetic field B in a force line varies as $n_i = n_e = n_0/K$, where n_0 is the initial density, and $K = B_m/B$ is the expansion degree. Electrons, unlike ions, are locked in a deep potential well and follow a Maxwellian distribution, whereas the density at a given point conforms to the Boltzmann law $n_e = n_0 \exp(-e\varphi/T_e)$. Equating ion and electron densities yields

$$\varphi = \frac{T_e}{e} \ln K.$$

The electron flux along a magnetic field line at a point with potential φ depends on the number of electrons surmounting the potential barrier:

$$J_e \approx n_0 V_{Te} \exp\left(-\frac{e\varphi}{T_e}\right) = n_0 \frac{V_{Te}}{K},$$

where V_{Te} is the electron thermal velocity. At the same time, the ion flux is constant along the field line tube and is $J_i \approx n_0 V_{Ti}$, where V_{Ti} is the ion thermal velocity. Then, if the expansion degree $K_w = B_m/B_w$ in the vicinity of the wall amounts to $V_{Te}/V_{Ti} \approx \sqrt{m_i/m_e}$, most electrons are reflected back into the trap as a result of the potential jump in the expander, while electron and ion fluxes become equal in magnitude. It has been shown experimentally (Fig. 15) that electron temperature in this region drops sharply due to the accumulation of cold electrons that make up for the ion spatial charge. Qualitatively, the potential profile in the expander looks like this: it first shows a sharp jump between the mirror and the surface where $K \approx \sqrt{m_i/m_e}$; thereafter, it remains practically unaltered, but in the end experiences another jump on the plasma damp surface kept at a zero potential.

Thus, energy electrons from the trap are almost fully locked in the electrostatic well of the ambipolar potential. The energy of the electrons that reach the wall is low, and the secondary cold electrons knocked out of the wall cannot enter the trap, since their magnetic moment is conserved and the magnetic field jump between the wall and the mirror under typical conditions amounts to $\sim 10^3$ or more. As a result, the electron heat flux from the trap to the end wall is suppressed. This effect was demonstrated in an experiment with a movable central segment of the wall [105]. The surface of this segment was covered with an oxide layer and heated to the temperature at which the emission density of cold electrons reached ~ 1 A cm^{-2}. When the field value at the segment surface was lower than the magnetic mirror field by a factor of $\sqrt{m_i/m_e} \approx 40$ and more, the segment position did not affect the ambipolar potential jump in the expander (Fig. 16). The potential jump shown in this figure was normalized to $4.8T_e$, i.e., its theoretical value at the large expansion degrees. Parameters of plasma under heating by the injection of hydrogen atom beams did not depend on the wall position either. If, however, the wall was so close to the mirror that the field ratio was lower than 40, the potential jump decreased. Likewise, plasma electron temperature in the central part fell, which suggests a strongly enhanced electron heat flux toward the end wall.

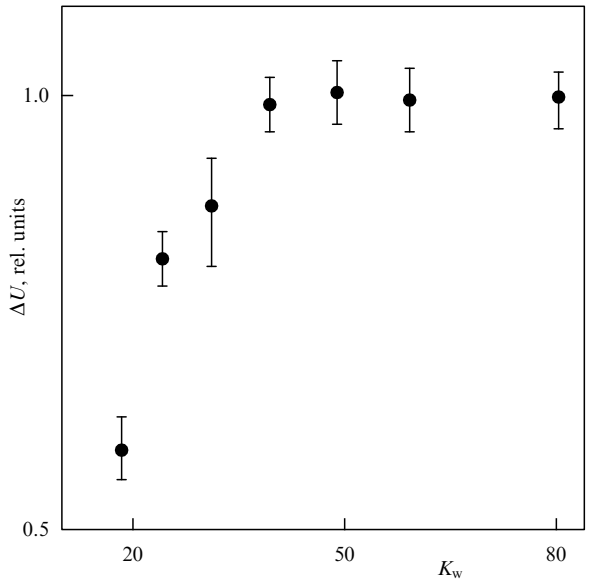

Figure 16. Potential jump in the expander with a movable segment of the end wall depending on the expansion degree.

6. Magnetohydrodynamic stability of plasma heated by neutral beams

6.1 Stabilization by expanders

The injection of neutral beams into the plasma resulted in the accumulation of fast ions oscillating between the turning points near magnetic mirrors and in the heating of electrons in the trap. The behavior of the target plasma during heating and fast ion accumulation was substantially different in those regimes with unfavorable and favorable field line curvatures in the expansion tanks.

In the former case, plasma density sharply decreased and its profile symmetry was significantly broken. Although the plasma source continued to operate during the first 600 μs after the onset of injection and the plasma remained stabilized by the end walls, its linear density over the cross section underwent sharp chaotic changes. The density decreased and its profile broadened substantially within 100–200 μs after the source was switched off. The plasma temperature sharply fell, too, probably because the plasma strongly interacted with radial limiters in the trap central section.

If the field line curvature was favorable for stability, the plasma showed a quite different behavior. Density perturbations were much less pronounced and unaccompanied by such dramatic declines. Nevertheless, the behavior of the target plasma at a high injection power (over 200 kW) showed features characteristic of MHD-unstable confinement regimes. They were manifested as displacements of the plasma column and broadening of the density profile during heating. Simultaneously, plasma density in the halo leaning upon the limiters along the field lines increased 3–5-fold during a 1-ms pulse injection; this was accompanied by greatly increased energy losses from the target plasma, so that its temperature was several times less than expected based on calculations. Electron temperature was rapidly saturated at a level of 15–20 eV, when the plasma consumed a beam power in excess of 300 kW. At a heating power of ~ 100 kW, plasma temperature increased over the entire duration of an injection pulse.

Detailed measurements of the plasma energy balance during heating and calculations of stability margin dynamics showed that the plasma overcomes the MHD-stability threshold in the course of fast ion accumulation. This phenomenon is related to the decrease in the rate of energy transfer from fast ions to plasma electrons with increasing electron temperature. As a result, fast ion pressure in the trap central section grows more quickly than plasma pressure in the expander, depending on the electron temperature of the target plasma. Assuming for simplicity that the target plasma and fast particles make an identical contribution to the average unfavorable field line curvature, it is possible to write down the stability condition in the form of the following inequality: $W_p(\Delta_s - 1) \geqslant W_f$, where W_p and W_f denote energy content in fast ions and target plasma, respectively. The instant of time when this inequality no longer holds as fast particles continue to accumulate corresponds to a transition through the stability boundary.

It was assumed for the purpose of analysis of experimental beam injection data that the plasma rigid-body displacement mode, $m = 1$, becomes unstable. In the paraxial approximation for this mode taking account of its structure, the perturbation of plasma energy upon displacement ξ_0 in the trap central plane is given by [106, 107]

$$\delta W = -\pi B_{\min} \xi_0^2 \int \psi \, \mathrm{d}\psi \int \frac{\mathrm{d}l}{B^2 r} \, \kappa \, \frac{\partial (P_\perp + P_{||})}{\partial \psi} \,, \qquad (4)$$

where ψ is the magnetic flux. Assuming that the angular distribution of the injected ions is rather narrow, it is possible to evaluate with reasonable accuracy their contribution to energy perturbation associated with flute rising. Naturally, this contribution is proportional to the energy content in fast particles. For an isotropic plasma with a clear-cut boundary, integral (4) is trivially calculated if the shape of the field lines is optimal (3); it equals $\delta W = -\xi_0^2 W_f / 4 l_m^2$. The favorable contribution to stability determined by plasma pressure behind the mirrors is proportional to the energy content in the target plasma. In other words, it can be concluded in the approximations being used that plasma parameters at the stability boundary in W_f and W_p coordinates correspond to a certain straight line. In measurements, the instant of transition across the stability boundary was recorded as a moment at which the time derivative of plasma energy content disappeared. The data presented in Fig. 17 correspond to stability margin $\Delta_s \approx 3$ that qualitatively agrees with measurements of Δ_s in a cold plasma.

The maximum plasma temperature rose from 15 to 20–25 eV upon beam injection into a GDT stabilized by the expander, while the injection power decreased, the duration increased, and (all other conditions being equal) the magnetic field underwent strengthening. Taken together, these changes give indirect evidence that limitations on temperature and plasma energy content during heating are related to the process of system transition into an unstable state initiated by beam injection and the impossibility of maintaining the density of the warm target plasma in these experiments.

6.2 Cusp-stabilized plasma

Experiments described in the preceding section demonstrate convincingly that plasma in the axisymmetric GDT can be efficiently stabilized using end expansion tanks with a favorable curvature of field lines. At the same time, the measured stability margin is not critical if compared with

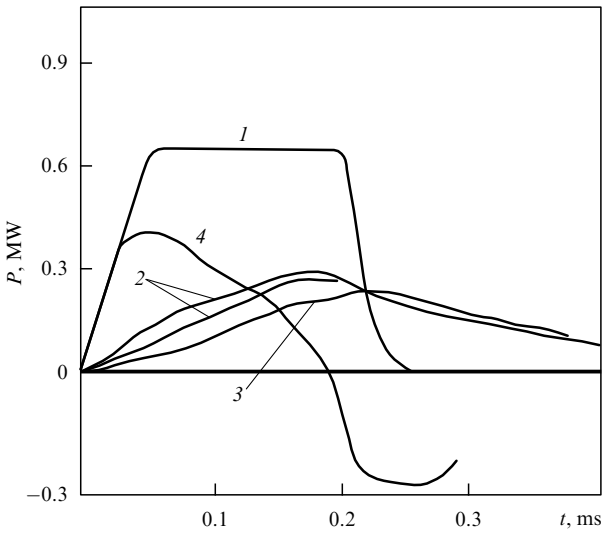

Figure 17. Energy fluxes in the plasma during beam injection: *1* — injection power, *2* — power transferred from fast ions to electrons, *3* — charge exchange power losses of fast ions, and *4* — time derivative of fast ion energy content.

the expected one. There is a pretty high degree of theoretical uncertainty as regards the choice of the upper limit in the stability integral corresponding to the contribution from the segments of magnetic field lines near the end wall. This allows, by reasonably changing the limitation on the value of $\kappa\rho_i$ in the expander, reaching fairly good agreement between observed and predicted stability margins. At the same time, this quantity depends on the contribution from the lines of force with a weak magnetic field. For this reason, the contribution cannot be arbitrarily great once limitations are imposed on the following characteristics: the line slope to the axis in the expander, permissible curvature radius ($\kappa\rho_i \leqslant 1$), the minimal expander radius (longer than ρ_i), maximum β in the expander, and the condition that the plasma flow velocity not exceed the Alfvén speed.

The problem of the maximum possible stability margin is discussed in Ref. [75]. For the power-law shape of the field lines, the favorable contribution from an 'optimal' expander is 1.5–2 times greater than the predicted one [36] used earlier to evaluate the stability margin; it equals $\Delta_s \propto l_m/\rho_i R$ up to the unessential factor. All the parameters in this expression are rigidly fixed, which accounts for the narrow range of stability margin variations in the expander. These considerations predetermine interest in the search for MHD stabilizers capable of assuring a wider stability margin.

To increase the stability margin, it was proposed in Ref. [108] to use an end cell (a cusp) in which plasma is confined in the adiabatic region in the gas dynamic regime. It was expected that the transit particles flowing out of the central cell and passing all the way through the cusp would be captured in it due to rare collisions and retained between the axial and radial maxima of the magnetic field. As a result, the total plasma pressure in the expander would greatly increase in comparison to that of the transit plasma. To estimate pressure inside the cusp, both its halves were assumed to be filled with plasma having a constant temperature equal to that in the trap central section in a given field line.

Plasma density and pressure were determined from the balance of particles flowing out of the trap into the cusp and issuing from it through the annular slit and the outer magnetic mirror: $P = (P_0/B_m)/(2/B_r + 1/B_m^*)$, where B_m is the magnetic field in the inner (inlet) mirror, B_r is the magnetic field in the ring slit, and B_m^* is the magnetic field in the outer (outlet) mirror of the cusp (end cell). When filling the cusp with the plasma flux from the trap, the possibility of two stationary states corresponding to supersonic and subsonic plasma flow regimes should be taken into consideration. The latter regime has been realized in the experiments described below.

Efficient plasma stabilization by the cusp implies the fulfillment of several conditions. First, the radius of curvature of magnetic field lines in the maximum pressure gradient region must be much longer than the ion Larmor radius. Therefore, the design of the cusp stabilizer limited the radius of curvature to $0.3/\rho_i$. The second condition requires suppression of drift instabilities responsible for the marked broadening of the density profile in the ring slit in experiments [109–111]. For this purpose, cusp parameters were chosen such that plasma size in this region was greater than four ion Larmor radii calculated based on the electron temperature. This condition resulted in the cusp slit radius being smaller than $r_p^2/4\rho_i$, where r_p is the plasma radius at the entrance to the cusp. Moreover, plasma pressure in the cusp did not have to strongly disturb the shape of the field lines through the diamagnetic effects. With this in mind, an upper limit was placed on the relative plasma pressure in the cusp, $\beta \leqslant 0.3$. Calculations taking account of these limitations showed that the stability margin for a field line with a radius of 10 cm in the trap center was ~ 8, with the mirror ratio being $R = 75$. At a plasma density in the trap of 10^{14} cm^{-3} and electron temperature of 50 eV, the β value in this line of force was 0.1, and $\kappa\rho_i \leqslant 0.2$.

The measured plasma pressure in the casp outside the region of ion adiabaticity was shown to be fairly well described by equations for the particle longitudinal flow balance. Energy perturbations in the flute displacement of the target plasma with isotropic pressure were estimated with the use of the data reported in Ref. [35]. Energy perturbations for the global mode were calculated taking account of nonparaxiality as

$$\delta W_p = \pi B_{min} \xi_0^2 \int \psi \, d\psi \left(\frac{\partial P}{\partial \psi} \frac{\partial U}{\partial \psi} + \gamma \frac{P}{U} \left(\frac{\partial U}{\partial \psi} \right)^2 \right), \qquad (5)$$

where $U = \int dl/B$.

The specific volume of magnetic flux tubes between axial and end mirrors was the first to be calculated, together with its derivative for the real geometry of the cusp coils. Then, plasma pressure in the cusp and its derivative with respect to the magnetic flux were found from experimental data. Finally, integral (5) was calculated, with the lower limit of integration corresponding to the boundary of the adiabatic region in the cusp. A cutoff in the integral at the lower limit introduced a certain error into the calculations. However, the contribution to energy perturbations in the cusp for weak magnetic flows was rather small due to its bi-logarithmic character: $\delta W_p \propto \ln\ln 1/\psi$. Energy perturbation for fast ions was calculated as described by Kruskal and Oberman [112] taking account of magnetic field paraxiality in the trap central section.

The plasma energy lifetime was determined dividing maximum energy content in the plasma by the heating power, and the particle lifetime was obtained from the density reduction rate in the trap at the same point in time.

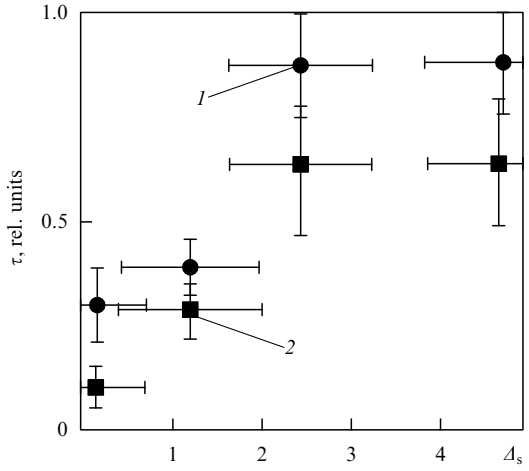

Figure 18. Plasma confinement time as a function of stability margin: *1* — particle confinement time, and *2* — energy confinement time.

Energy content was saturated after its maximum was reached, which suggested enhanced plasma loss. The states with different plasma pressures in the cusp (hence, with different stability margins) were realized as follows. The states with $\Delta_s \leqslant 2$ were obtained at the mirror ratio $R = 50-80$, that with $\Delta_s = 2.5$ at $R = 27$, and regimes with $\Delta_s \geqslant 2.5$ by injecting plasma from an additional gun installed in the outer axial mirror of the cusp to fill its entire near-axial region. Heating caused rapid accumulation of fast ions in the central section of the trap and thereby decreased the stability margin. Due to this, for the above values of $\Delta_s \geqslant 1$, the initial Δ_s value at the stability boundary amounted to 100 and higher.

Figure 18 illustrates the dependences of particle's lifetime and energy in the trap center on the calculated stability margin. Experimental data were normalized to the respective calculated lifetimes of the plasma flowing out through the mirrors. It can be seen that the lifetime begins to decrease for $\Delta_s \leqslant 2$ in accordance with the general picture of dynamic transition through the stability boundary associated with fast ion accumulation.

Interestingly, in experiments with low plasma temperatures (2–3 eV) due to the absence of additional heating, the plasma showed behavioral features characteristic of unstable decay regimes. In such cases, plasma movements in the trap central section and in the cusp were uncorrelated, probably owing to the influence of plasma finite conductivity, which makes possible the development of the so-called resistive ballooning mode in the central cell [98].

The use of the cusp for MHD-driven instability stabilization allowed a significant enhancement of plasma parameters in the GDT. |In doing so, the plasma remained stable at a significantly higher power of injected beams (up to 4.2 MW), a duration of 1.1 ms, and an injection energy of 13–17.5 keV. As a result, parameter β increased to 15–20%, while plasma temperature reached 90–110 eV. The density of fast ions with a mean energy of 5–8 keV at the turning points was $\sim 10^{13}$ cm^{-3} [113]. An important factor that further promoted enhancement of plasma parameters was the use of titanium arc-discharge evaporators to deposit Ti film over the inner wall of the vacuum chamber prior to each shot [114].

Simultaneously, major deficiencies in the use of the cusp stabilizer have come to light in concrete experimental conditions, when plasma parameters turn out to be essentially nonstationary. Despite the markedly enhanced stability margin in comparison with that in expansion tanks at moderate initial Δ_s values, the stability limit was reached in the course of fast ion accumulation. The involvement of an additional plasma gun in the cusp further increased stability margin Δ_s and kept plasma stable over the entire duration of the injection pulse. However, the growth of plasma temperature in these regimes was limited by a heat leak through the electron channel to the end wall, where plasma guns were installed. In later experiments, the effects of nonstationarity associated with pulsed injection of the beams were partly compensated by gas feeding into the space between the magnetic mirror and the turning point for fast ions.

6.3 Stabilization by sheared azimuthal rotation

Subsequent experiments designed to study mechanisms of transverse transfer in GDTs were in a way prompted by the results obtained at the HIEI facility in Kyoto, Japan [115, 116]. The main technique employed by the authors to stabilize flute oscillations was ponderomotive stabilization making use of the pressure gradient of cyclotron waves induced in plasma. HIEI is an axisymmetric open-ended magnetic trap in which the application of a positive potential to the radial limiters caused a sharp decline in transverse losses. It was hypothesized that the observed suppression of drift turbulence and reduction of a transfer rate were due to the strongly sheared azimuthal rotation of the plasma ($\partial\omega_E/\partial r$, where ω_E is the azimuthal rotation frequency, and r is the plasma radius) in the crossed magnetic and electric fields near a limiter.

The theory predicts that irregular plasma rotation with a shear may interfere with the development of unstable MHD perturbations [117]. The mechanism of favorable influence of differential rotations on plasma stability with respect to flute perturbations can be qualitatively characterized as follows. Let a rising flute in plasma enter the region with a strong shear flow (in this case, the attribute 'strong' implies that the characteristic time taken by plasma layers to complete a turn relative to each other through an angle on the order of unity is comparable to or less than the time needed for instability to form. Then, the shear flow causes the flute to 'smear' over the azimuth (i.e., decreases azimuthal gradients) and can significantly reduce the instability growth rate.

Suppression of MHD-driven instability in a nonuniformly rotating plasma has been observed in many experiments. Specifically, this method was applied in experiments at the PSP-2 device (PSP — Plasma in Crossed Fields) in Novosibirsk [118]; the plasma obtained had a temperature of ~ 10 keV at a density of $\sim 10^{18}$ m^{-3}. The Maryland Centrifugal eXperiment (MCX) [119] at the University of Maryland (USA) demonstrated that instability can be tamed when the shear in rotational flow velocity in crossed $\mathbf{E} \times \mathbf{B}$ fields is larger than the growth rate of MHD perturbations. The GAMMA-10 experiments (Tsukuba, Japan) also showed that a large enough rotational flow velocity shear, either spontaneous or generated by end electrodes and local ECR heating, is responsible for the suppression of MHD and drift modes [120].

Plasma rotation in the GDT was controlled by a method similar to that used at the HIEI facility. Specifically, potentials of the radial limiters arranged in the central section of the trap behind the turning point of fast ions and those of the ring segments of the plasma dump in the expander

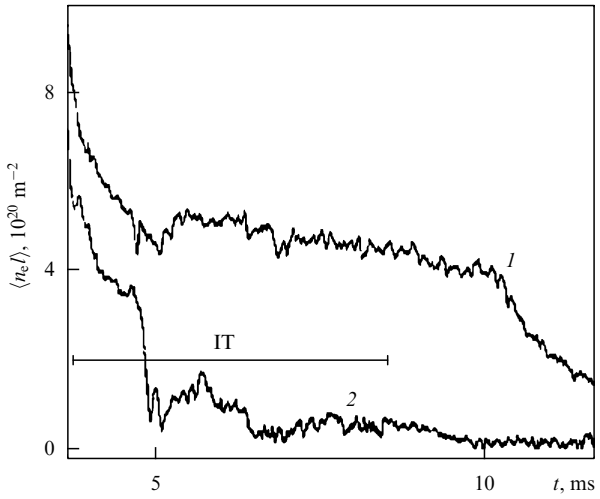

Figure 19. Plasma line density in the trap with (curve *1*) and without (curve *2*) a voltage supply to the limiters; IT — injection time of atomic beams.

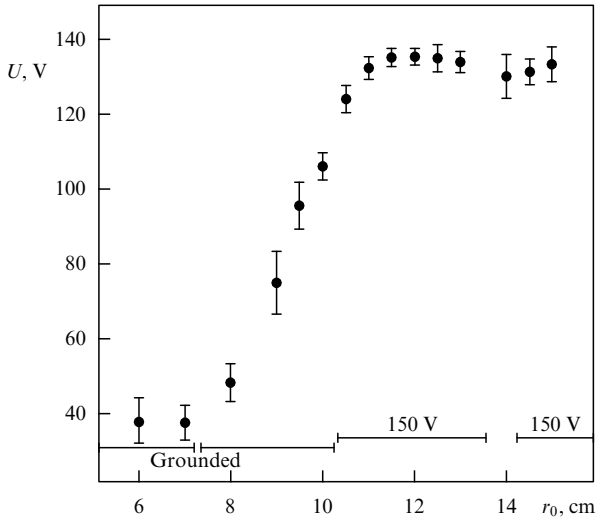

Figure 20. Radial profile of the floating potential near a limiter.

were either generated by external power supply or grounded. The potentials were chosen so as to form a region with a strong radial electric field at the plasma edge, resulting in a vortex at the plasma boundary, i.e., a plasma flow in crossed $\mathbf{E} \times \mathbf{B}$ fields with a strong shear. The influence of such plasma rotation on the transverse transfer proved even more pronounced than in the HIEI experiments. In fact, if the potential of the limiters exceeded a certain value on the order of the electron temperature, transverse losses became relatively small. This effect is demonstrated in Fig. 19 demonstrating the temporal behavior of the plasma line density in different operating regimes of the facility.

To recall, the transverse losses remained small even if the field line curvature in the expanders was close to zero. Therefore, cusp coils were not switched on in further experiments, so that the lines of force in the end cells were almost straight and their average curvature was unfavorable for stability. Plasma heating and confinement in beam injection experiments were evaluated at an injection pulse duration up to 5 ms. The energy of an injected beam ranged 23–25 keV, and the power incident on the plasma varied within 3.5–5.4 MW (Table 5). Radial plasma transfer was controlled by applying a voltage to the plasma damp segments and the radial limiter in the central solenoid. It is under such regimes that the maximum plasma energy stored and maximum diamagnetism were achieved.

The characteristic potential radial profile observed in experiment is presented in Fig. 20. Measurements were made when the radial limiter and the outer ring segment of the plasma damp were exposed to a potential of around 130 V with respect to the grounded inner segments. The potential dynamics are well described by the theoretical dependence found in Ref. [117]. The width of the profile in the theoretical model was related to the development of Kelvin–Helmholtz instabilities in the plasma. The presence of ions with a large Larmor radius stabilized all MHD modes but those with $m \approx 1$. The growth of unstable perturbations was restricted by their nonlinear saturation due to their connection with the end system and generation of transverse currents in the vortex region. As a result, the plasma is confined in a dead zone of the vortex flow without appreciable transverse displacements and losses on the walls. However, the theoretical mechanism of nonlinear saturation of unstable mode amplitudes operates for $\langle \rho_i \rangle \ll a$, whereas in experiment $\langle \rho_i \rangle \approx a$. Further progress in the theory is needed to enable more rigorous research in this field.

Table 5. Plasma parameters in GDTs obtained with the use of different MHD stabilizers.

Parameter	Expander [99]	Cusp [113]	Plasma rotation [121]
Central magnetic field, T	up to 0.22	up to 0.22	up to 0.3
Mirror magnetic field, T	2.5–15	2.5–15	2.5–15
Primary plasma density, m^{-3}	$(1.5-7) \times 10^{19}$	4.5×10^{19}	$(3-6) \times 10^{19}$
Plasma radius in trap center, cm	≈ 6.5	5–10	6–7
Electron temperature, eV	up to 25	up to 110	up to 250 ($\sim 10^3$ with additional ECR heating)
Energy of injected deuterium or hydrogen beams, keV	15	15–16	24–25
Duration of injection, ms	1.2	1.2	5
Total injection power, MW	—	up to 4	up to 5.7
Injection angle, degrees	45	45	45
Fast ion density at stagnation points, m^{-3}	$\approx 1 \times 10^{18}$	$\approx 0.4 \times 10^{19}$	$\approx (5-7) \times 10^{19}$
Mean curvature in MHD stabilizers relative to the curvature in the central section without regard for fast ion contribution	1.5–2	≈ 8 at $R = 25$	—
Mean fast ion energy, keV	—	5–8	≈ 10
Maximum local β	≈ 0.07	≈ 0.1	up to 0.6

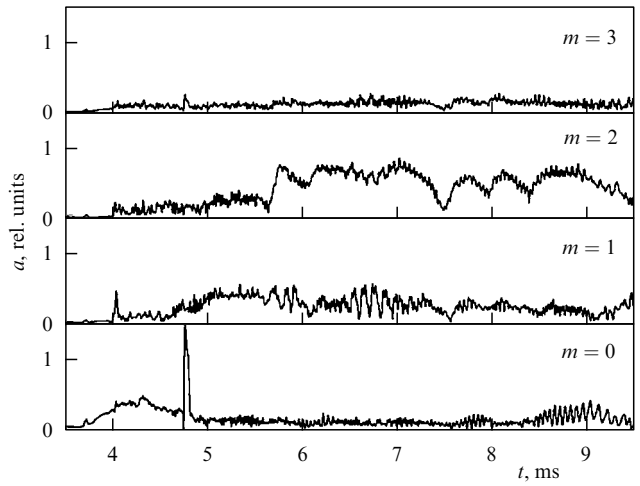

Figure 21. Temporal behavior of amplitudes of flute perturbation azimuthal harmonics with different numbers. The starting time of neutral beam injection is 3.7–4 ms.

Plasma activity induced by the injection of neutral beams was examined using an array of magnetic sensors installed at different azimuths and along the axis in the central section of the trap. The typical shape of the signals from the sensors following their treatment in the form of flute modes is depicted in Fig. 21. As expected, the azimuthal mode spectrum is dominated by modes with $m \approx 1$. The presence of a mode with $m = 0$ is largely due to plasma heating. The amplitudes of higher-order modes with $m \geqslant 3$ are much lower than those of modes with $m = 1, 2$, corresponding to plasma displacement as a whole and elliptical distortion of the plasma cross section. It follows from Fig. 21 that harmonic amplitudes do not grow exponentially as they were supposed to, bearing in mind that the weighted mean curvature of the magnetic field lines is unfavorable for stability; in fact, they grow only up to a certain value. An interesting feature is the high amplitude of the $m = 2$ mode, which is several times higher than that of the $m = 1$ mode, suggesting an important role of nonlinear mechanisms [117].

Analysis of experimental data obtained in different regimes permitted us to arrive at a number of qualitative conclusions. First, only one mode, either $m = 1$ or $m = 2$, is routinely dominated in the oscillation spectrum at each instant of time. In this case, the frequency spectrum turns out to be rather narrow, but the frequency maximum may fall in a sufficiently broad frequency range from 10 to 50 kHz. Second, plasma rotation frequency at a fixed m increases together with the voltage applied to a limiter. Third, fast 'switching' between modes was observed in a series of experiments. As this takes place, the product of frequency by number of the dominating mode changes weakly. Thus, in the experiment demonstrated in Fig. 21 the switching occurred after a lapse of 5.7 ms. An $m = 1$ mode with a frequency of 40 kHz was observed before the time indicated, and an $m = 2$ mode with a frequency of 20 kHz after above time.

It is useful to compare measured frequencies of experimental flute perturbations with characteristic growth rates of MHD-unstable modes and plasma rotation frequency. The MHD instability growth rate in GDTs, when the stabilizing cells are switched off, can be estimated as $\gamma_{\mathrm{MHD}} \sim \omega_{\mathrm{MHD}} \approx V_{\mathrm{Ti}}\,\kappa/a \approx V_{\mathrm{Ti}}/L$. Ion velocity V_{Ti} should be described in terms of fast ion parameters that make a major contribution to plasma pressure and have a mean energy of 10 keV. Then, if the trap length is assumed to be determined by the field line curvature ($L \approx 6-7$ m), the characteristic MHD-perturbation growth rate is $f_{\mathrm{MHD}} = \omega_{\mathrm{MHD}}/2\pi \approx 30$ kHz. The plasma rotation velocity is a function of drift in the crossed fields with velocity $V_{\mathrm{drift}} = cE/B$ and plasma radius $a \approx 10$ cm. The rotation frequency is $f_{\mathrm{rot}} \approx 15-30$ kHz on the estimation that $E = 30-50$ V cm^{-1}, corresponding to the potential profile shown in Fig. 21. These estimates are close enough to the experimentally observed perturbation frequencies. In addition, since the rotation frequency is very similar to the estimated flute instability growth rate, it can be concluded that the rotation of plasma markedly affected its behavior in the experiment under consideration.

As was noted before, GDT experiments with maximum plasma relative pressure have been carried out in the regime with the magnetic field of around 0.3 T in the central cross section and plasma vortex rotation at the periphery [64]. Figure 22 presents the time dependence of plasma diamagnetism for this regime. Its comparison with the results of simulations gives evidence that transverse losses did not play a significant role in plasma energy balance. The density of fast ions with a mean energy of 10–12 keV at the turning point was as high as 5×10^{19} m^{-3}, or much higher than target plasma density $(1.5-3) \times 10^{19}$ m^{-3} in the GDT central cross section. This difference accounted for the appearance of ambipolar potential peaks and an appreciable reduction in longitudinal plasma losses from the near-axial region. Diagnostics based on the Stark effect showed that the magnetic field decreased compared with the vacuum one by almost $\Delta B/B_{\mathrm{v}} = 0.3$, resulting in the relative plasma pressure $\beta \approx 0.6$.

In another series of experiments with the magnetic field in the trap center as low as 0.25 T, the radial profile $\Delta B/B_{\mathrm{v}}$ was measured in the projection onto the central plane of the trap cross section (Fig. 23) together with the plasma density profile [122]. It follows from Fig. 23 that diamagnetic field expulsion amounted to $\Delta B/B_{\mathrm{v}} = 0.2$ on the plasma axis, so that the relative pressure in this case reached $\beta \approx 0.4$. A distinctive feature of the density profile thus obtained is its small width (about 7 cm at the 1/e level in the projection onto the central plane of the GDT cross section). Notice that it is only slightly bigger than the Larmor radius of fast deuterium ions ($\rho_{\mathrm{i}} \approx 5.6$ cm) calculated for the mean energy of fast ions.

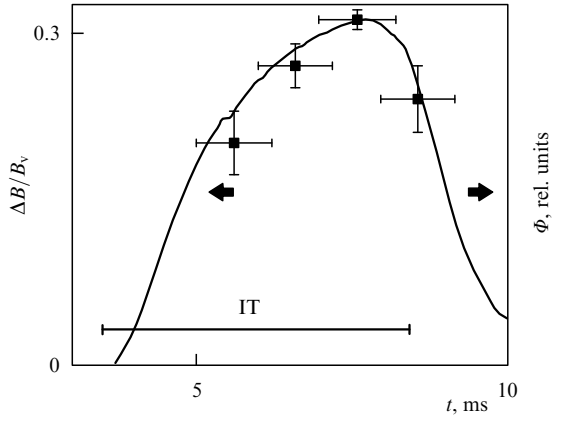

Figure 22. Time dependence of the relative change in the magnetic field and plasma diamagnetism; IT — injection time of neutral beams.

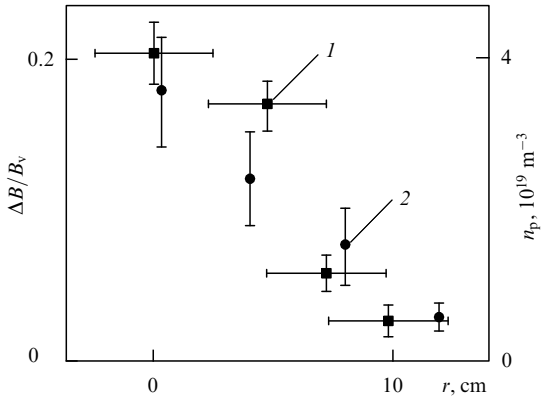

Figure 23. Radial profiles: *1* — relative changes of the magnetic field, and *2* — plasma density.

The formation of so narrow a radial density profile of fast ions cannot be accounted for by peripheral losses or the narrow profile of neutral beam capturing. The concrete mechanism behind transition into this state remains to be elucidated. It may be related to the flowing of ion current between the plasma near-axial region and the periphery, where the plasma potential becomes negative after the negative potential is applied to the radial limiter. The application of the electric potential with an opposite sign did not lead to the formation of the narrow density profile of fast ions.

Experiments with an expansion tank and cusp functioning as stabilizers showed that the relative plasma pressure grew almost linearly with increasing energy content of fast ions up to ~ 0.2; transition into regimes with plasma vortex rotation at the periphery resulted in further enhancement of energy content also accompanied by a linear in time alteration of relative pressure, but with a higher proportionality coefficient.

Measurements of plasma energy balance upon injection of neutral beams gave evidence that elevated plasma losses are lacking up to the regimes with maximum $\beta = 0.6$. However, even for $\beta > 0.4$ plasma perturbations develop. These perturbations can be roughly divided into two groups: one comprising slow perturbations with a frequency of ~ 10 kHz, and the other including fast perturbations with megahertz frequencies. Perturbations of the former type are characteristically exemplified by spontaneous redistributions of plasma pressure along the central GDT solenoid and by perturbations of the shape of the plasma cross section [123]. The plasma behavior in these cases can be illustrated by signals from diamagnetic loops located in the trap center with the mirror ratio $R = 1$ and in the turning point for fast ions with the mirror ratio $R = 2$ (see ovals in Fig. 24). Plasma pressure redistribution along magnetic field lines follows its buildup, so that the signal from the loop in the center sharply increases within the time interval between 4.1 and 4.2 ms, but respectively decreases at the turning point.

The accumulation of fast ions was accompanied by saw-like relaxation oscillations of signals from diamagnetic loops (Figs 25, 24). Transverse plasma pressure redistribution was studied with a set of magnetic sensors arranged parallel to the trap axis. Figure 25b presents perturbation of the radial component of the magnetic field with respect to its value in a vacuum; the main contribution to the perturbation comes from fast ions. Broadening of its longitudinal profile is most noticeable at a time instant of around 5.5 ms, when the first dip in the diamagnetic signal becomes apparent. At this time,

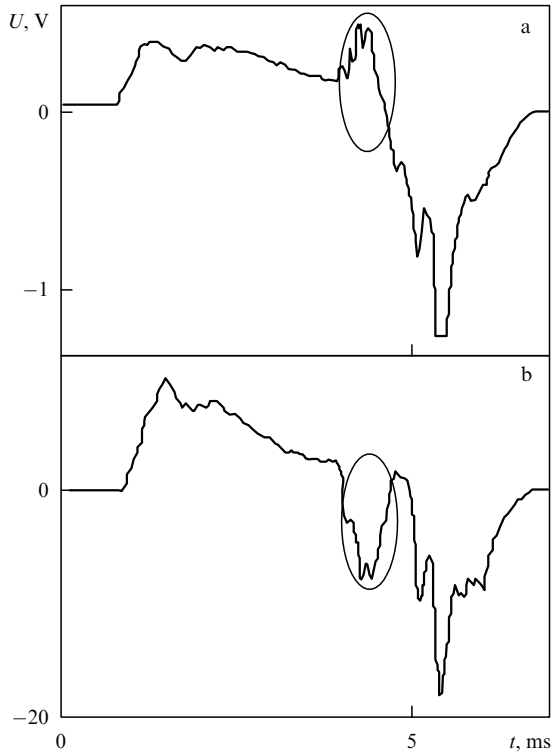

Figure 24. Diamagnetic loop signals: (a) in the central cross section ($R = 1$), and (b) near the turning point ($R = 2$).

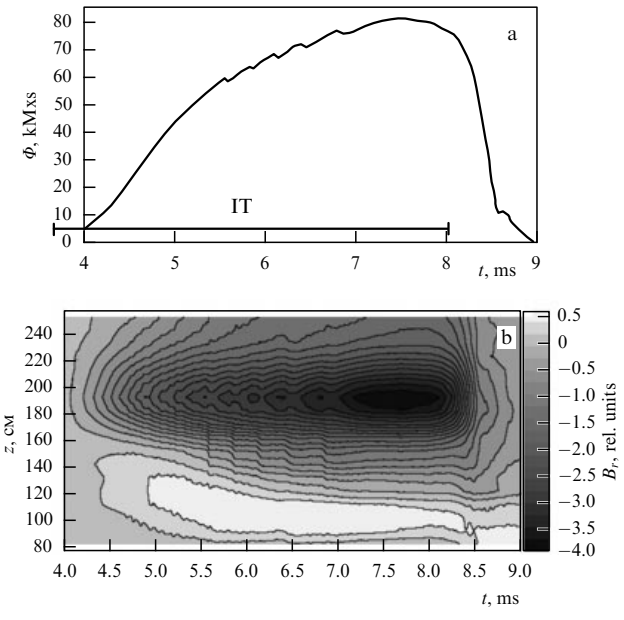

Figure 25. Time dependence of diamagnetic signal at $R = 2$ (a), and the dependence of the radial magnetic field perturbation on time and longitudinal coordinate (b); IT — injection time, and kMxs units — kilomaxwells.

the perturbation amplitude of the radial magnetic field decreases near the center of the ion turning region (the dark region near $z = 190$ cm narrows), while it grows at the edge of this region (the level lines in the range $z = 140-160$ cm take the form of a 'step' as they shift toward smaller z). At the same time, the dips in the diamagnetic signals were accompanied by bursts of HF oscillations at a frequency of around 1 MHz (Fig. 26). The measured characteristics of the plasma HF

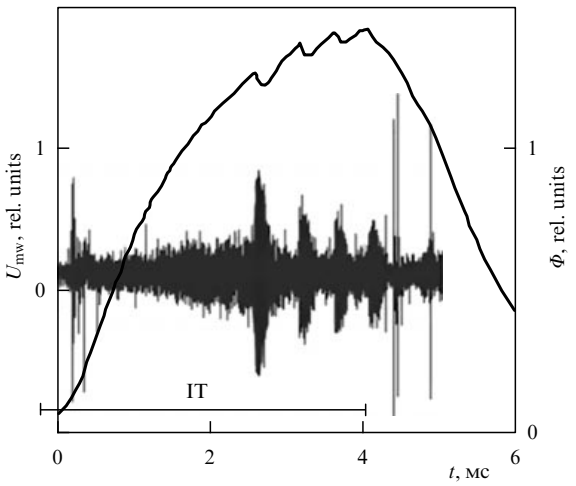

Figure 26. Microwave probe and diamagnetic loop signals versus time at $R = 2$; IT — injection time.

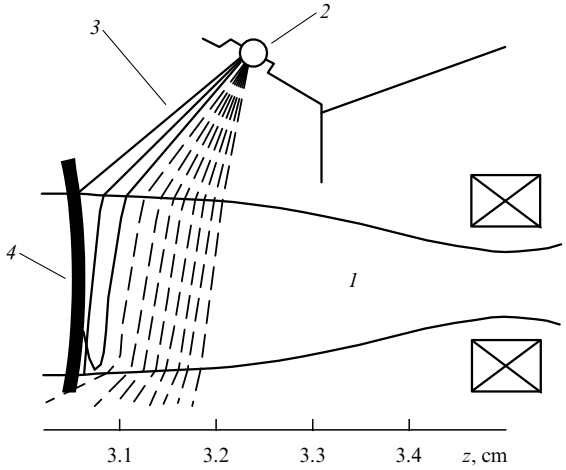

Figure 27. Schematic of ECR heating: *1* — plasma, *2* — radiation input zone, *3* — trajectories of captured (solid lines) and uncaptured (dashed lines) rays, and *4* — resonant surface.

oscillations suggest that they correspond to bursts of the Alfvén ion cyclotron (AIC) instability considered in the Introduction [124].

A theoretical description of this instability type for open-ended magnetic traps with oblique beam injection is presented in Ref. [125]. It is worthwhile to note that the development of AIC instability in GDTs, in contrast to many other systems, does not cause substantial losses of fast ions [126], because only a small group of them having a maximum energy (i.e., fast ions freshly captured from heating neutral beams) is responsible for the wave buildup. It is enough to only slightly increase (by $\sim 1^\circ - 2^\circ$) the angular spread of such particles to saturate oscillations, whereas the pitch angle must be changed by $\sim 40^\circ$ to make such particles enter the loss cone.

7. Plasma microwave heating experiments

To increase electron temperature and decrease the energy loss rate for injected ions, the GDT facility was equipped with a plasma heating system operating at the electron cyclotron resonance frequency. Two 54.5-GHz gyrotrons were used (an equivalent to resonance in a field of 1.95 T). Radiation was brought into cyclotron resonance zones located symmetrically with respect to the trap center. The total gyrotron power amounted to 0.9 MW and was comparable to the electron heating power generated in electron–fast ion collisions (1–1.5 MW).

An example of radiation power input is schematically shown in Fig. 27. The wave was introduced from the side of a strong magnetic field and directed to the absorption zone as a result of refraction at the plasma boundary and subsequent complete internal reflection from the plasma–vacuum interface. A wave traveling in the plasma is captured in the plasma waveguide and directed into the ECR zone. Such a waveguide forms because the wave movement in the weakening magnetic field is associated with the growth of longitudinal refractive index, while the angle between the wave vector and the magnetic field becomes smaller due to refraction. In this region behind the fast ion reflection point, the plasma parameters are such that the condition $\omega_{pe} < \omega_{ce}$ is fulfilled and the wave frequency $\omega \sim \omega_{ce}$. The refractive index of an extraordinary wave whose polarization rotates in the direction of electron rotation in the magnetic field and the absorption of which results in electron heating has, in the cold plasma approximation, a peculiarity in the magnetic field

$$B = \frac{m_e c}{e} \frac{\omega}{\sqrt{1 + \omega_{pe}^2 \sin^2\theta/(\omega^2 - \omega_{pe}^2)}},$$

corresponding to the upper hybrid resonance frequency. The square of the wave refractive index is positive behind the upper hybrid resonance point closer to the magnetic mirror, and the wave can propagate.

Thus, a wave entering plasma from the side of a strong magnetic field does not reach the nontransparency region but finds itself at the cyclotron resonance point, where it must be absorbed. It is known, however, that the wave changes the direction of polarization at the cyclotron resonance point and is incapable of resonant interaction with electrons [127]. If the plasma electron temperature is high enough, a rather wide region with a polarization component rotating in the direction of electrons appears near the resonance point. Electrons moving along the magnetic field can effectively interact with the wave by virtue of Doppler frequency shift. The experiments were conducted at the characteristic values of $\beta_e = V_{Te}/c \sim 10^{-2}$ and $\omega_{pe}^2/\omega_{ce}^2 \sim 0.3$ to fulfill the condition $\omega_{pe}^2/\beta_e\omega_{ce}^2 \gg 1$. In this case, when the angle between the magnetic field and the wave propagation direction was $\theta \approx 1$, the extraordinary wave absorption length was rather small [128]:

$$l \sim \frac{c}{\omega}\frac{\omega_{pe}^2}{\omega_{ce}^2}\left(1 - \frac{\omega_{pe}^2}{\omega_{ce}^2}\right)^{-2} \sim 6 \text{ cm}.$$

If angle θ is so small that the inequality $\theta^3 \leqslant \beta_e$ is satisfied, the wave further damps out near resonance and is absorbed at length

$$l \sim c\left(\frac{\beta_e}{\omega_{pe}^2\omega_{ce}}\right)^{1/3} \sim 0.03 \text{ cm}.$$

Injection of gyrotron radiation into the plasma raised its electron temperature (Fig. 28), caused enhancement of plasma diamagnetism, and increased the flux of neutrons from the D–D reaction (Fig. 29) due to the decrease in energy losses of the injected fast ions. Further optimization of

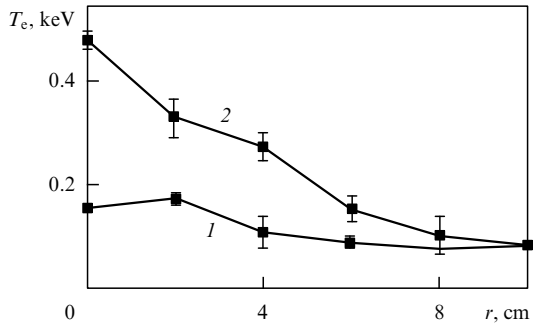

Figure 28. Radial profile of electron temperature: *1* — without ECR heating, and *2* — with 300-kW ECR heating.

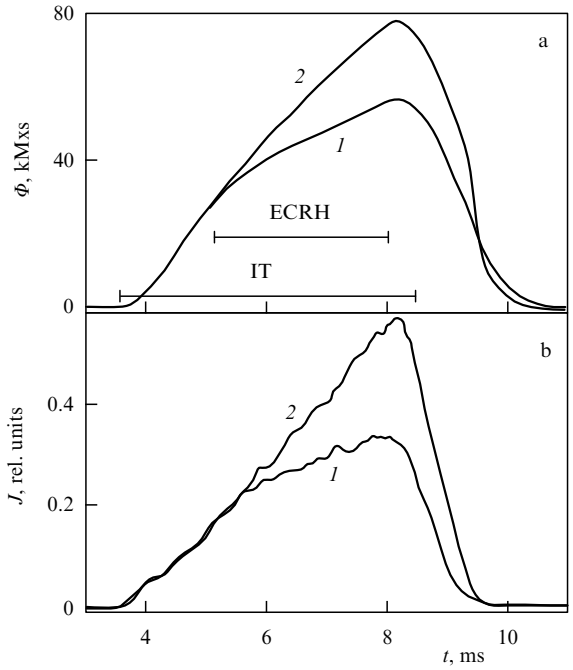

Figure 29. Temporal evolution of plasma diamagnetism (a) and neutron flux (b): *1* — without ECR heating, and *2* — with 300-kW ECR heating; IT — injection time, ECRH — ECR heating time, and kMxs units — kilomaxwells.

heating conditions and microwave power input to the plasma allowed its electron temperature on the trap axis to be elevated to about 1 keV [44, 45].

8. Conclusions

The GDT experiments have successfully demonstrated that plasma MHD-driven instabilities in an axisymmetric gas dynamic trap can be stabilized by external cells with a favorable curvature of magnetic field lines. Two types of such stabilizers were studied: the expander, and the cusp; they were filled with the plasma flowing out of the trap. Also investigated was plasma confinement with small transverse losses under conditions when the weighted mean curvature of magnetic field lines was unfavorable for stability. In this case, the plasma was confined inside the vortex flow with a large velocity shear at the periphery, maintained by applying potentials to radial limiters and segments of the end plasma dump.

Experiments showed that losses of heat from the trap due to electron thermal conductivity can be greatly suppressed by decreasing the magnetic field between the mirror and the trap end. The drop of plasma density in the expanding flux behind the mirror results in a deep potential well for electrons in the central solenoid. As a consequence, most electrons from the trap central section cannot reach the wall. In addition, the expansion of the flux behind the mirror causes the potential profile to flatten in the outside part of the end cells. Under these conditions, cold electrons emitted from the wall where the magnetic field is much weaker than the mirror field can not enter the central solenoid and cool the plasma it contains. Therefore, it can be concluded that axial heat losses from the central solenoid of a GDT are largely determined by plasma flux through the mirrors.

The experiments also demonstrated that the measured longitudinal particle and energy fluxes from the trap at low temperatures ($T \leqslant 50$ eV) agree with those predicted by the gas dynamic model of plasma flow in magnetic mirrors [106]; at higher temperatures, the observed flows are consistent with the theoretical ones described by the collisionless model [105]. Plasma heating by the injection of neutral beams is associated with the predominance of axial losses in the energy balance, while the fraction of transverse losses is below 15%. In such regimes, electron temperature in the GDT amounting to 250 eV depends on the balance of energy transferred from fast ions to electrons and plasma outflow through the magnetic mirrors. Additional ECR heating of the plasma in the central section of the trap raises the electron temperature to almost 1 keV.

Confinement of fast ions injected into the trap in its central section at an angle of 45° to the axis is fairly well described in terms of classical electron drag mechanisms and ion–ion scattering. AIC instability develops in the plasma only in the case of attaining its maximum relative pressure [124]. However, neither enhanced fast ion losses nor an appreciable broadening of the turning point region is observed in the presence of developed instability.

Successful operation of GDTs with $\beta \leqslant 0.6$, the classical behavior of fast injected ions, and the possibility of heating electrons in the trap to about 1 keV taken together provide a solid basis for considering GDTs a prototype of a D–T neutron source with a neutron flux up to 2 MW m^{-2} annually consuming around 0.1 kg of tritium. Such a source faces no serious physical, engineering, or technological limitations. Importantly, the energy spectrum of GDT neutrons is identical to that of fusion neutrons in the ITER and future DEMO power plants; it satisfies all requirements imposed on neutron sources for materials testing to be used in thermonuclear reactors.

Apart from exploitation of GDTs as a neutron source, they can be used to study the interaction of strong plasma fluxes with the surfaces of engineering materials due to the high energy content in the plasma and strong magnetic fields in the mirrors. A plasma flux through the mirror is easy to vary widely by altering the injection power and gas feeding regime, giving the opportunity to model conditions in the divertors of future tokamak reactors. For example, the placement of the model wall of a tokamak reactor in the mirror is likely to increase the thermal flux power up to hundreds of megawatts/m^2. Then, the energy of electrons and ions interacting with the wall may be 100–120 eV, i.e., enough to simulate real working conditions of a major disruption in the tokamak. Experiments can be based on the use of hydrogen, deuterium, and tritium plasma, as shown recently in a GDT study [129]. The tungsten target was installed near

the end magnetic mirror, the power density of the plasma flux was higher than 160 MW m^{-2}, and electron temperature in the trap center was maintained at the level of 140 eV.

For all that, the plasma was nonstationary under the conditions of the above experiments. Suffice it to say that its electron temperature in stable regimes continued to grow over the entire duration of an injection pulse. This means that the operating time of the GDT facility must be further extended to reach stationary conditions (e.g., to 20 ms or more at the electron temperature of $\sim$ 200 eV). There are plans to realize such regimes in the course of the device modification. Specifically, the Budker Institute of Nuclear Physics (Novosibirsk) plans to construct a stationary plasma confinement system, a gas dynamic multiple-mirror trap (GDMT) [130]. The GDMT concept is based on the employment of multiple-mirror end solenoids for more efficient suppression of axial plasma losses than in the prototype GDT. Naturally, such a facility must have a superconducting magnetic system and a duration of microwave or beam injection heating of around 100 s if the stationary conditions are to be created. The primary objective of the GDMT experiment will be to test the concept of a stationary multiple-mirror fusion D–T reactor. Given that the problem of stability at high plasma pressure and temperature is successfully solved, a GDMT-based thermonuclear reactor may be designed in the distant future making use of new 'aneutronic' fuels, such as D–He^3, He^3–He^3, and p–B^{11}.

Acknowledgments

The authors greatly acknowledge the unfailing support of D D Ryutov, whose pioneering research work (in cooperation with V V Mirnov and their colleagues) laid the foundation for the concept of gas dynamic traps and GDT-based neutron sources. An important contribution to the studies of GDT physics was made by other researchers affiliated with the Budker Institute of Nuclear Physics, RAS including A V Anikeev, P A Bagryansky, A D Beklemishev, I A Kotel'nikov, A A Lizunov, E I Soldatkina, and A L Solomakhin, to whom the authors extend their sincerest thanks for detailed discussions of various aspects of GDT physics. Thanks are also due to K Noack (Helmholtz-Zentrum Dresden-Rossendorf, HZDR, Germany), B V Robouch (Frascati Research Centre of the Italian National Agency for New Technologies, Energy and Sustainable Economic Development, Italy), U Fischer and A Moslang (Karlsruhe Institute of Technology, KIT, Germany), and D DenHartog (University of Wisconsin, Madison, USA) for insightful discussions and assistance, T Simonen (University of California, Berkeley, USA) for his interest in this work, constructive criticism, and comprehensive support, and M V Ivantsivskii, A I Gorbovskii, and A Kh Amirov for assistance in manuscript preparation

This study was supported by a grant from the Russian Science Foundation (project No. 14-50-00080).

References

1. Budker G I *Plasma Physics and the Problem of Controlled Thermonuclear Reactions* Vol. 3 (Ed. M A Leontovich) (New York: Pergamon Press, 1959) p. 1; Translated from Russian: in *Fizika Plazmy i Problema Upravlyaemykh Termoyadernykh Reaktsii* Vol. 3 (Ed. M A Leontovich) (Moscow: Izd. AN SSSR, 1958) p. 3, the work done in 1954
2. Post R F, in *Proc. of the Second United Nations Intern. Conf. on the Peaceful Uses of Atomic Energy, Geneva, 1 – 13 September 1958* Vol. 32 (Geneva: United Nations, 1958) p. 245
3. Yushmanov E E *Sov. Phys. JETP* **22** 409 (1966); *Zh. Eksp. Teor. Fiz.* **49** 588 (1965)
4. Sivukhin D V *Reviews of Plasma Physics* Vol. 5 (Ed. M A Leontovich) (New York: Consultants Bureau, 1967); Translated from Russian: in *Voprosy Teorii Plazmy* Iss. 5 (Ed. M A Leontovich) (Moscow: Atomizdat, 1967) p. 439
5. Mirnov V V, Ryutov D D, in *Itogi Nauki i Tekhniki. Ser. Fizika Plazmy* (The Progress of Science and Technology. Ser. Plasma Physics) Vol. 8 (Moscow: VINITI SSSR, 1988) p. 77
6. Ioffe M S, Kadomtsev B B *Sov. Phys. Usp.* **13** 225 (1970); *Usp. Fiz. Nauk* **100** 601 (1970)
7. Rosenbluth M N, Longmire C L *Ann. Physics* **1** 120 (1957)
8. Mirnov V V, Ryutov D D *Sov. Tech. Phys. Lett.* **5** 279 (1979); *Pis'ma Zh. Tekh. Fiz.* **5** 678 (1979)
9. Dory R A, Guest G E, Harris E G *Phys. Rev. Lett.* **14** 131 (1965)
10. Rosenbluth M N, Post R F *Phys. Fluids* **8** 547 (1965)
11. Post R F, Rosenbluth M N *Phys. Fluids* **9** 730 (1966)
12. Post R F "Mirror confinement and its optimization", UCRL-70681 (1967)
13. Gerver M J *Phys. Fluids* **19** 1581 (1976)
14. Berk H L et al., in *Plasma Physics and Controlled Nuclear Fusion Research, 1976. Proc. of the Sixth Intern. Conf., Berchtesgaden, West Germany, October 6 – 13, 1976* Vol. 3 (Vienna: IAEA, 1977) p. 147
15. Coensgen F H et al. *Phys. Rev. Lett.* **35** 1501 (1975)
16. Simonen T C et al. *Phys. Rev. Lett.* **50** 1668 (1983)
17. Rosenbluth M N (General Atomic Div., General Dynamics Corp., San Diego, CA) "Microinstabilities", Report RISO-18 (Roskilde: Riso National Laboratory, 1960) p. 189
18. Sagdeev R Z, Shafranov V D *Sov. Phys. JETP* **12** 130 (1961); *Zh. Teor. Eksp. Fiz.* **39** 181 (1960)
19. Watson D C *Phys. Fluids* **23** 2485 (1980)
20. Casper T A, Smith G R *Phys. Rev. Lett.* **48** 1015 (1982)
21. Katsumata R et al. *Jpn. J. Appl. Phys.* **31** 2249 (1992)
22. Dimov G I, Zakaidakov V V, Kishinevskii M E *Sov. J. Plasma Phys.* **2** 326 (1976); *Fiz. Plazmy* **2** 597 (1976)
23. Budker G I, Mirnov V V, Ryutov D D *JETP Lett.* **14** 212 (1971); *Pis'ma Zh. Teor. Eksp. Fiz.* **14** 320 (1971)
24. Dimov G I *Phys. Usp.* **48** 1129 (2005); *Usp. Fiz. Nauk* **175** 1185 (2005)
25. Post R F *Nucl. Fusion* **27** 1579 (1987)
26. Ryutov D D, Stupakov G V *JETP Lett.* **26** 174 (1977); *Pis'ma Zh. Teor. Eksp. Fiz.* **26** 186 (1977)
27. Cheremnykh P A et al. *Prib. Tekh. Eksp.* (5) 226 (1976)
28. Mirnov V V, Nagorny V L *Voprosy Atom. Nauki Tekh. Ser. Termoyad. Sintez* (9) 40 (1984)
29. Kotel'nikov I A et al. "Matematicheskaya model' istochnika neitronov na osnove gazodinamicheskoi lovushki" ("Mathematical model of GDT-based neutron source"), Preprint (Novosibirsk: Inst. of Nuclear Physics of the Siberian Branch of the Acad. of Sci. USSR, 1990); http://www.inp.nsk.su/activity/preprints/files/1990_105.pdf
30. Wang Q et al. *IEEE Trans. Appl. Conduct.* **25** 4603505 (2015)
31. Bagryansky P A et al. *Fusion Eng. Des.* **70** 13 (2004)
32. Fowler T K, Logan B G *Comments Plasma Phys. Controlled Fusion* **2** 167 (1977)
33. Baldwin D E, Logan B G *Phys. Rev. Lett.* **43** 1318 (1979)
34. Zhil'tsov V A, Skovoroda A A, Shcherbakov A G, in *Trudy Vsesoyuz. Soveshchaniya po Otkrytym Lovushkam, Moskva, 19–21 Oktyabrya 1989* (Proc. of the All-Union Meeting on Open Traps, Moscow, 19–21 October 1989) (Moscow, 1989) p. 143
35. Ryutov D D, Stupakov G V *Sov. J. Plasma Phys.* **12** 815 (1986); *Fiz. Plazmy* **12** 1411 (1986)
36. Casey J A et al. *Phys. Fluids* **31** 2009 (1988)
37. Lane B et al. *Nucl. Fusion* **27** 277 (1987)
38. Post R F *Fusion Sci. Technol.* **39** 25 (2001)
39. Post R F *Fusion Sci. Technol.* **43** 195 (2003)
40. Post R F et al. *Fusion Sci. Technol.* **47** 49 (2005)
41. Li X Z, Kesner J, Lane B *Nucl. Fusion* **25** 907 (1985)
42. Arsenin V V, Chuyanov V A *Sov. Phys. Usp.* **20** 736 (1977); *Usp. Fiz. Nauk* **123** 83 (1977)
43. Beklemishev A D *Fusion Sci. Technol.* **59** (1T) 90 (2011)
44. Bagryansky P A et al. *Nucl. Fusion* **55** 053009 (2015)
45. Bagryansky P A et al. *Phys. Rev. Lett.* **114** 205001 (2015)

46. Anikeev A V et al. *Proc. 23th EPS Conf. Plasma Physics Controlled Fusion* **20C** 688 (1996)
47. Bagryansky P A et al. *Trans. Fusion Technol.* **35** (1T) 79 (1999)
48. Yurov D V, Prikhodko V V *Phys. Usp.* **57** 1118 (2014); *Usp. Fiz. Nauk* **184** 1237 (2014)
49. Sorokin A et al. *Rev. Sci. Instrum.* **81** 02B108 (2010)
50. Davydenko V I, Ivanov A A, Shul'zhenko G I *Plasma Phys. Rep.* **41** 930 (2015); *Fiz. Plazmy* **41** 1004 (2015)
51. Deichuli P *Rev. Sci. Instrum.* **86** 113509 (2015)
52. Davydenko V *Rev. Sci. Instrum.* **87** 02B303 (2016)
53. Belchenko Yu et al. *Rev. Sci. Instrum.* **87** 02B133 (2016)
54. Sorokin A V et al. *Tech. Phys.* **61** 1004 (2016); *Zh. Tekh. Fiz.* **86** (7) 46 (2016)
55. Robouch B V et al. *Proc. 16th IEEE/NPSS Symp.* **2** 1131 (1995)
56. Fischer U, Moeslang A, Ivanov A A *Trans. Fusion Technol.* **35** (1T) 160 (1999)
57. Fischer U, Donne M D, in *Proc. 4th Intern. Symp. on Fusion Nuclear Technology, Tokyo, Japan, April 6–11, 1997*
58. Ehrlich K, Daum E, in *Proc. of the IAEA Workshop on Intense Neutron Sources, Karlsruhe, 21–23 September 1992*; KfK Report 5296 (1994)
59. IFMIF CDA Team "International Fusion Materials Irradiation Facility. Conceptual Design Activity", Report RT/ERG/96/11, December (Ed. M Martone) (Frascati: ENEA, 1996); *Nucl. Instrum. Meth.* **145** (1) (1977)
60. Jung P et al. *J. Nucl. Mater.* **232** 186 (1996)
61. Abdou M *Fusion Eng. Des.* **27** 111 (1995)
62. Ryutov D D et al. *J. Fusion Energy* **17** 253 (1998)
63. Kruglyakov E P *Fusion Sci. Technol.* **39** (1T) 57 (2001)
64. Bagryansky P A *Tran. Fusion Sci. Technol.* **59** (1T) 31 (2011)
65. Deichuli P, private communication
66. Ryutov D D *AIP Conf. Proc.* **1442** 247 (2012)
67. Lotov K V, Ivanov A A *Plasma Phys. Control. Fusion* **42** 1077 (2000)
68. Konkashbaev I K, Landman I S, Ulinich F R *Sov. Phys. JETP* **47** 501 (1978); *Zh. Eksp. Teor. Fiz.* **74** 956 (1978)
69. Ryutov D D *Fusion Sci. Technol.* **47** 148 (2005)
70. Anikeev A V et al. *Plasma Phys. Rep.* **25** 775 (1999); *Fiz. Plazmy* **25** 842 (1999)
71. "Accelerator and spallation target technologies for ADS applications (A status report)", OECD/NEA Report 5421 (Paris: OECD Publ., 2005); https://www.oecd-nea.org/science/docs/pubs/nea5421-accelerator.pdf
72. Möllendorff U et al. "A nuclear simulation experiment for the International Fusion Materials Irradiation Facility (IFMIF)", Report FZKA-6764 (Karlsruhe: Forschungszentrum Karlsruhe, 2002); http://digbib.ubka.uni-karlsruhe.de/volltexte/fzk/6764/6764.pdf
73. Postupaev V V et al. *Fusion Eng. Des.* **106** 29 (2016)
74. Beklemishev A D *Phys. Plasmas* **22** 103506 (2015)
75. Bagryansky P A et al. *J. Nucl. Mater.* **265** 124 (1999)
76. Anikeev A V et al. *Plasma Phys. Rep.* **20** 176 (1994); *Fiz. Plazmy* **20** 192 (1994)
77. Korepanov S A et al. *Trans. Fusion Technol.* **35** 345 (1999)
78. Berezovskii E L et al. *Sov. J. Plasma Phys.* **6** 760 (1980); *Fiz. Plazmy* **6** 1385 (1980)
79. Tammen H F et al. *Plasma Phys. Rep.* **20** 158 (1993)
80. Abdrashitov G F et al. *Rev. Sci. Instrum.* **72** 594 (2001)
81. Anikeev A V et al., in *1998 Intern. Congress on Plasma Physics and 25th EPS Conf. on Controlled Fusion and Plasma Physics, Praha, June 29–July 3, 1998* Vol. 22C (Ed. P Pavlo) (1998) p. 1498
82. Bagryansky P A et al. *Rev. Sci. Instrum.* **74** 1592 (2003)
83. Lizunov A A *Rev. Sci. Instrum.* **82** 086105 (2011)
84. Lizunov A A et al. *Rev. Sci. Instrum.* **86** 126109 (2015)
85. Davydenko V I, Ivanov A A *Rev. Sci. Instrum.* **75** 1809 (2004)
86. Medley S S et al. *Rev. Sci. Instrum.* **79** 011101 (2008)
87. Davydenko V I et al. *Plasma Phys. Rep.* **23** 396 (1997); *Fiz. Plazmy* **23** 427 (1997)
88. Prikhodko V V, Murakhtin S V *Trans. Fusion Sci. Technol.* **47** (1T) 315 (2005)
89. Hinton F L, Rosenbluth M N *Nucl. Fusion* **22** 1547 (1982)
90. Kotel'nikov I A, Roslyakov G V, Ryutov D D *Sov. J. Plasma Phys.* **13** 227 (1987); *Fiz. Plazmy* **13** 403 (1987)
91. Ivanov A A et al. *Phys. Plasmas* **1** 1529 (1994)
92. Molvik A W et al. *Phys. Fluids* **27** 2711 (1984)
93. Rosenbluth M N, Krall N A, Rostoker N *Nucl. Fusion* (1) 143 (1962)
94. Itatani R, Takeno H, Yasaka Y, in *Plasma Physics and Controlled Nuclear Fusion Research, 1986* Vol. 2 (Vienna: IAEA, Vienna,1987) p. 273
95. Anikeev A V et al. *Plasma Phys. Control. Fusion* **34** 1185 (1992)
96. Anikeev A V et al. *Plasma Phys. Control. Fusion* **37** 1239 (1995)
97. Berk H L et al., in *Plasma Physics and Controlled Nuclear Fusion Research, 1990* Vol. 2 (Vienna: IAEA, 1991) p. 289
98. Tsidulko Yu A "Rezistentnaya balonnaya moda v gazodinamicheskoi lovushke" ("Resistant ballooning mode in GDT"), Preprint (Novosibirsk: Inst. of Nuclear Physics of the Siberian Branch of the Acad. of Sci. USSR, 1992)
99. Bagryansky P A et al., in *Plasma Physics and Controlled Nuclear Fusion Research, 1990* Vol. 2 (Vienna: IAEA, 1991) p. 655
100. Bagryansky P A "Uderzhanie dvukhkomponentnoi plazmy s vysokim β v gazodinamicheskoi lovushke" ("Confinement of two-component plasma with high β in GDT"), Thesis of a Dissertation for the Degree of Doctor of Phys.-Math. Sci. (Novosibirsk: Budker Institute of Nuclear Physics of the RAS, 2001)
101. Molvik A W, Casper T A, Futch A H *Nucl. Fusion* **30** 1061 (1990)
102. Molvik A W et al. *Phys. Rev. Lett.* **48** 742 (1982)
103. Anikeev A V et al. *Nucl. Fusion* **40** 753 (2000)
104. Maximov V V *Nucl. Fusion* **44** 542 (2004)
105. Anikeev A V et al. *Plasma Phys. Rep.* **25** 775 (1999); *Fiz. Plazmy* **25** 842 (1999)
106. Bagryansky P A "MGD-ustoichivost' teploi plazmy v gazodinamicheskoi lovushke" ("MHD-stability of warm plasma in GDT"), Thesis for Cand. Phys.-Math. Sci. (Novosibirsk: Budker Institute of Nuclear Physics of the RAS, 1990)
107. Ryutov D D et al. *Phys. Plasmas* **18** 092301 (2011)
108. Ivanov A A et al., in *Trudy Vsesoyuz. Soveshchaniya po Otkrytym Lovushkam, Moskva, 19–21 Oktyabrya 1989* (Proc. of the All-Union Meeting on Open Traps, Moscow, 19–21 October 1989) (Moscow, 1989) p. 15
109. Haines M G *Nucl. Fusion* **17** 811 (1977)
110. Pastukhov V P *Sov. J. Plasma Phys.* **6** 549 (1980); *Fiz. Plazmy* **6** 1003 (1980)
111. Ilgisonis V I, Pastukhov V P, Preprint IAE-3495 (Moscow: IAE, 1981)
112. Kruskal M D, Oberman C R *Phys. Fluids* **1** 265 (1958)
113. Anikeev A V et al. *Phys. Plasmas* **4** 347 (1997)
114. Anikeev A V et al., in *Proc. of 23th EPS Conf. on Controlled Fusion and Plasma Physics, Bournemouth, UK, 1995, Conf. Papers* Vol. 19C, Pt. IV, p. 193
115. Sakai O, Yasaka Y, Itatani R *Phys. Rev. Lett.* **70** 4071 (1993)
116. Sakai O, Yasaka Y, Itatani R, in *Proc. of Intern. Conf. on Open Plasma Confinement Systems for Fusion* (Ed. A Kabantsev) (Novosibirsk, 1993) p. 197
117. Beklemishev A D et al. *Fusion Sci. Technol.* **57** 351 (2010)
118. Volosov V I *Plasma Phys. Rep.* **35** 719 (2009); *Fiz. Plazmy* **35** 782 (2009)
119. Ellis R *Bull. Am. Phys. Soc.* **53** (14) 75 (2008) papers CP6 92 to 97
120. Cho T et al. *Fusion Sci. Technol.* **51** (2T) 11 (2007)
121. Ivanov A A et al. *Fusion Sci. Technol.* **57** 322 (2010)
122. Ivanov A A et al. *Phys. Rev. Lett.* **90** 105002 (2003)
123. Prikhodko V V et al. *Trans. Fusion Sci. Technol.* **59** (1T) 94 (2011)
124. Zaytsev K V et al. *Fusion Sci. Tech.* **63** (1T) 346 (2013)
125. Tsidulko Yu A, Chernoshtanov I S *Plasma Phys. Rep.* **40** 955 (2014); *Fiz. Plazmy* **40** 1074 (2014)
126. Anikeev A V et al. *Plasma Phys. Rep.* **41** 773 (2015); *Fiz. Plazmy* **41** 839 (2015)
127. Shafranov V D *Reviews of Plasma Physics* Vol. 3 (Ed. M A Leontovich) (New York: Consultants Bureau, 1963); Ed. M A Leontovich) (Moscow: Gosatomizdat, 1963) p. 34
128. Akhiezer A I et al. *Plasma Electrodynamics* (Oxford: Pergamon Press, 1975); Translated from Russian: Akhiezer A I (Ed.) *Elektrodinamika Plazmy* (Moscow: Nauka, 1974)
129. Soldatkina E I, Arakcheev A S, Bagryansky P A *Fusion Eng. Des.* **88** 3084 (2013)
130. Beklemishev A et al. *AIP Conf. Proc.* **1442** 147 (2012)